Scaling unlocks broader generation and deeper functional understanding of proteins

Aadyot Bhatnagar[*,†] **Sarthak Jain**[*] **Joel Beazer**[*] **Samuel C. Curran**[*]

Alexander M. Hoffnagle[*] **Kyle Ching**[*] **Michael Martyn**[*] **Stephen Nayfach**[*]

Jeffrey A. Ruffolo[*,†] **Ali Madani**[*,†]

Abstract

Generative protein language models (PLMs) are powerful tools for designing proteins purpose-built to solve problems in medicine, agriculture, and industrial processes. Recent work has trained ever larger language models, but there has been little systematic study of the optimal training distributions and the influence of model scale on the sequences generated by PLMs. We introduce the ProGen3 family of sparse generative PLMs, and we develop compute-optimal scaling laws to scale up to a 46B-parameter model pre-trained on 1.5T amino acid tokens. ProGen3's pre-training data is sampled from an optimized data distribution over the Profluent Protein Atlas v1, a carefully curated dataset of 3.4B full-length proteins. We evaluate for the first time in the wet lab the influence of model scale on the sequences generated by PLMs, and we find that larger models generate viable proteins for a much wider diversity of protein families. Finally, we find both computationally and experimentally that larger models are more responsive to alignment with laboratory data, resulting in improved protein fitness prediction and sequence generation capabilities. These results indicate that larger PLMs like ProGen3-46B trained on larger, well-curated datasets are powerful foundation models that push the frontier of protein design.[1]

1 Introduction

Proteins are ubiquitous molecules that play a central role in most biological processes. They catalyze reactions, contribute to immune function, regulate cellular pathways, and facilitate the transport of other molecules. They enable solutions for multiple industries including therapeutics, diagnostics, agriculture, energy, and manufacturing. Until recently, we have been limited to finding relevant proteins in nature through serendipitous discovery. Techniques to engineer proteins for our desired purposes largely rely on laborious laboratory techniques that randomly mutate these initial hits in hopes of discovering a variant with enhanced function [3, 34]. Relying on these inherently random processes presents a major challenge to the bespoke design of proteins for specific use cases.

The dramatic reduction of DNA sequencing costs has enabled exponential growth in our ability to sample naturally occurring protein sequences that are the product of selective pressures over billions of years. Generative protein language models (PLMs) have emerged as powerful tools to learn the complex distribution of proteins found in nature, and their ability to design highly functional novel proteins has been experimentally verified for a wide range of applications [40, 45, 63, 68, 79, 80, 96].

[*]Profluent Bio, Inc.

[†]To whom correspondence should be addressed: {abhatnagar,jeff,ali}@profluent.bio

[1]Code and model weights are available at https://github.com/Profluent-AI/progen3.

Preprint.

The trajectory of these models mirrors those found in natural language processing (NLP) research. Earlier works in NLP demonstrated that larger models learn representations that can be fine-tuned to perform downstream tasks more effectively [30, 75, 100, 101], and elucidated the compute-optimal ways to scale up the size of both models and datasets to reap these benefits [43, 51]. Similarly, it has been shown that PLM embeddings implicitly capture notions of protein fitness that can be elicited in both supervised and unsupervised settings [15, 65, 69, 70, 90, 109], and recent work has derived compute-optimal scaling laws for PLMs [19].

However, a number of important questions have remained relatively under-explored in the PLM literature. Despite the rapidly accelerating growth of protein sequence datasets, little work has been done to determine the optimal data distributions for training ever larger PLMs [33]. While evaluations in NLP have shifted towards analyzing the sequences generated by LMs rather than properties of their embeddings [20, 23, 41], it is unclear how scale influences the proteins generated by PLMs, both computationally and experimentally. Finally, post-training strategies to align models with user-defined preferences have gained traction in both domains [74, 88, 106, 110], but the influence of an aligned PLM's scale on its performance has received only limited attention [40].

In this work, we introduce ProGen3, a family of autoregressive generative PLMs that leverages a sparse mixture of experts architecture [32, 56, 85] to improve efficiency while maintaining performance. To train ProGen3, we assemble the Profluent Protein Atlas v1 (PPA-1), a highly curated dataset of 3.4B full-length proteins and 1.1T amino acid tokens, and we optimize the data distribution for pre-training. We determine compute-optimal scaling laws for sparse PLMs and use them to scale ProGen3 up to a 46B parameter model trained on 1.5T tokens from PPA-1. Next, we evaluate for the first time in the wet lab the influence of model scale on the sequences generated by PLMs. We find that larger models generate viable proteins for much wider swaths of sequence space. Finally, we demonstrate both computationally and experimentally that models at all scales can be aligned with laboratory data for improved protein fitness prediction and sequence generation capabilities, and that the larger models receive the greatest lift from alignment. Taken together, these results present a clear case that larger protein language models trained on larger, well-curated datasets are more useful tools for a broad range of protein design challenges.

2 ProGen3

2.1 Architecture

ProGen3 is a family of autoregressive (AR) transformer based PLMs with a sparse mixture of experts (MoE) architecture that only activates 27% of its parameters per forward pass [32, 56, 85, 99] (Figure 1b). Models span 8 sizes ranging from 112M to 46B parameters, and all models have a context length of 8192 tokens. See Appendix C.1 for more details. Like prior work in NLP [29, 49], we find that for a fixed compute budget, sparse models meaningfully outperform dense ones (Appendix C.2).

A standard AR PLM enables *causal language modeling* (CLM), where users can generate proteins one amino acid at a time either from the N- to C-terminal, or from the C- to N-terminal [63, 68]. In addition to CLM, ProGen3 also performs *generalized language modeling* (GLM) to infill spans in the middle of a protein [6, 15, 35, 75, 83, 92]. It does so by replacing target spans with special sentinel tokens and placing those spans (preceded by their corresponding sentinel tokens) at the end of the sequence (Figure 1a). This capability allows users to redesign domains in the middle of a protein while attending to all surrounding residues. See Appendix C.3 for more details.

2.2 Training Data

To train ProGen3, we curate the Profluent Protein Atlas v1 (PPA-1), a dataset of 3.4B proteins and 1.1T amino acid tokens. PPA-1 draws from a wide range of genomic and metagenomic sources, and we apply multiple layers of quality filters to ensure the dataset is appropriate for pre-training a generative PLM. In particular, we exclude all protein fragments so we can train only on full protein sequences. PPA-1 is of similar scale and diversity to the OMG dataset [24]. It has a similar number of sequences as ESM3's dataset, but ESM3's dataset does include protein fragments [40]. It is also considerably larger than UniRef [91] and BFD [50, 87]. See Appendix B for more details.

While protein datasets are rapidly expanding, they have biases that influence the quality of PLMs trained on them [4, 31, 103]. Therefore, we aim to more rigorously study the impact of the train-

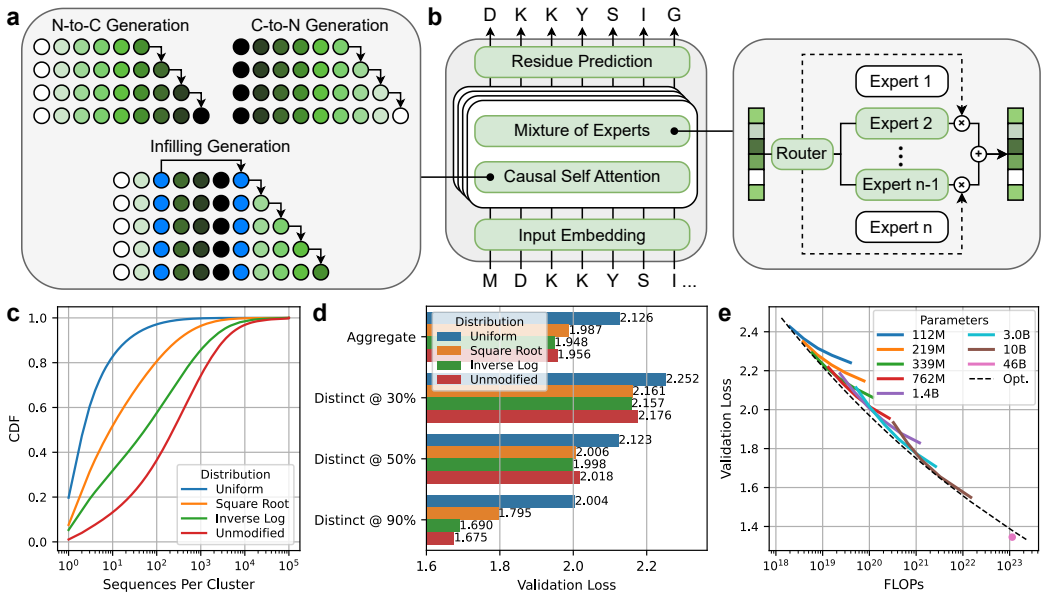

Figure 1: Determining the optimal data distribution and scaling laws to train ProGen3, a sparse generative PLM. (a) ProGen3 can generate proteins from the N- to C-terminal or from the C- to N-terminal. It can also generate spans in the middle of a protein. (b) ProGen3 is an autoregressive transformer with a sparse mixture of experts architecture. (c) Diversity of PPA-1 data distributions as measured by the CDF of 50% ID cluster sizes. (d) Validation losses of 1.4B parameter models trained on 80B tokens from different data distributions. (e) Validation losses of models with 112M to 46B parameters trained on 10B to 1.5T tokens from the Inverse Log distribution. "Opt." indicates the predicted losses for the compute-optimal configurations given by Equation 1.

ing distribution, an aspect which has received relatively less attention in prior PLM literature (Appendix A.2). We consider 4 different schemes of balancing data diversity over 50% ID clusters, which we refer to (in descending order of diversity) as Uniform, Square Root, Inverse Log, and Unmodified (Figure 1c). In each of these distributions, we respectively sample a 50% ID cluster of size n with probability proportional to 1 (equal probability), $\sqrt{n}$, $n/(1+\log n)$, and n (the natural sequence distribution). After sampling a 50% ID cluster, we sample a 90% ID sub-cluster from the same distribution, before sampling a sequence from that 90% ID sub-cluster uniformly at random.

To measure model generalization, we construct validation sets distinct from our training data at 30%, 50%, and 90% ID. Each x% ID validation set consists of 2.5M sequences distributed uniformly between X% ID clusters of sizes 1-10, 11-100, and 101-1000. The average loss thus avoids over-weighting highly represented parts of protein space and more accurately measures out-of-distribution generalization. We also average the losses on these sets to compute an aggregate validation loss.

Figure 1d shows the validation losses achieved by 1.4B parameter models trained for 80B tokens sampled from each distribution. For proteins close to our training data – distinct at 90% ID – training on the Unmodified distribution yields the best performance. The Inverse Log distribution is a close second, while the other two are considerably worse. However, training on the Inverse Log distribution yields the lowest loss for out-of-distribution sequences that are distinct from the training data at 50% and even 30% ID. We therefore train all subsequent models on the Inverse Log distribution.

Interestingly, training on the Uniform distribution, which is similar in spirit to de-replicating the training data at 50% ID, consistently obtains the worst performance on all validation sets. This suggests that PLMs can learn important signals from the frequencies with which related proteins occur in the data. However, some rebalancing can improve out-of-distribution generalization.

2.3 Scaling Up to a 46B Parameter Model

Given a fixed computational budget, scaling laws describe the optimal way to allocate pre-training resources between model size and dataset size [19, 43, 51]. They do so by predicting a model's loss L as a function of the number of parameters N and the number of tokens in the training dataset D. We fit a variant of the equation proposed by Kaplan et al. [51], $L(N, D) = \left(AN^{-\alpha/\beta} + BD^{-1}\right)^{\beta} + C$,

to the validation losses achieved by models spanning a wide range of parameter counts and dataset sizes. This equation can then be manipulated to yield a power law $N_{\text{opt}}(D) \propto D^{\beta/\alpha}$ which tells us the compute-optimal model size to pre-train on a dataset with D tokens.

We train models with 112M to 10B parameters for 10k to 500k steps (10B to 1T tokens, depending on batch size; see Appendix C.1). Because we use a cosine learning rate schedule, we train a separate model for each dataset size [43]. We plot their validation losses in Figure 1e and find

$$N_{\text{opt}}(D) = (2.462 \times 10^{-7})D^{1.479}. \tag{1}$$

This result for sparse AR PLMs agrees closely with Cheng et al. [19], who report that $N_{\text{opt}}(D) \propto D^{1.370}$ for dense AR PLMs. Equation 1 predicts that the optimal allocation for 1.1×10^{23} FLOPs is to train a 90B parameter model for 753B tokens. This model is predicted to achieve a validation loss of 1.376. We make the practical decision to instead train a 46B parameter model for 1.5T tokens because it is predicted to achieve a slightly higher validation loss of 1.397 but can be used for inference on 4xA100_40GB GPUs.

Interestingly, this 46B parameter model achieves a validation loss of 1.345, which lies below the predicted compute-optimal frontier (Figure 1e, bottom right). We had to increase the warmup period to stabilize the training for this model, which could explain the discrepancy, since a longer warmup improved the final training and validation losses of a 1.4B parameter model trained for 80B tokens (Appendix C.4).

3 Computational and Experimental Analysis of Model Generations

We have shown that scaling up the computational resources to pre-train PLMs predictably improves their validation losses for proteins both near and distant to their training data. In other words, larger models better represent the naturally occurring distribution of proteins. However, the implications of scaling on the generative capabilities of PLMs have largely gone unexplored by prior works. We focus on three models separated by three orders of magnitude in pre-training compute: ProGen3-339M (trained on 200B tokens with 1.2×10^{20} FLOPs), ProGen3-3B (trained on 500B tokens with 2.6×10^{21} FLOPs), and ProGen3-46B (trained on 1.5T tokens with 1.1×10^{23} FLOPs).

3.1 Larger PLMs generate more diverse proteins that express *in vitro*

From each model, we respectively generate 4M, 3M, and 2M sequences unconditionally using top-p sampling [44] with $p = 0.95$ and temperatures $T \in [0.5, 1]$. We then apply a series of quality filters to extract "protein-like" sequences. Because language models often generate repetitive sequences [44, 105], we first remove all sequences consisting of >25% low-complexity regions [36]; 95.5% of PPA-1 also passes this filter. We also require that generations include the appropriate termination token, and that they have >80% alignment coverage to any natural sequence in PPA-1 [2, 80]. Larger models generate more *valid* sequences that pass each of these quality filters, and scaling up from 339M to 3B especially reduces the number of repetitive generations (Figure 2a).

Next, we align each valid generation to the 30% ID cluster representatives in PPA-1 and say that it *covers* a cluster if it is >30% ID to the cluster representative with >90% alignment coverage. Note that a single generation can cover multiple clusters because a sequence can be >30% ID to multiple cluster representatives that are <30% ID to each other. Larger models generate sequences from a more diverse set of clusters than smaller models (Figure 2b). Moreover, the clusters covered by smaller models are almost entirely covered by larger models, while larger models generate sequences from a large number of clusters that are not covered by smaller models (Figure 2c).

To determine whether sampling more sequences would allow smaller models to generate from the clusters covered by larger models, we compute the average perplexities of the naturally occurring proteins in those clusters. If a given model assigns high perplexity to a cluster's naturals, it is unlikely to generate a sequence from that cluster. Figure 2d shows that larger models routinely generate from clusters that smaller models assign high perplexity, but not vice versa. This implies that larger models can cover all the clusters that smaller models generate from, but that some of the clusters covered by larger models are out-of-distribution for smaller models. This trend is partially explained by the fact that as models scale up, they become better at covering smaller clusters (Figure 2e).

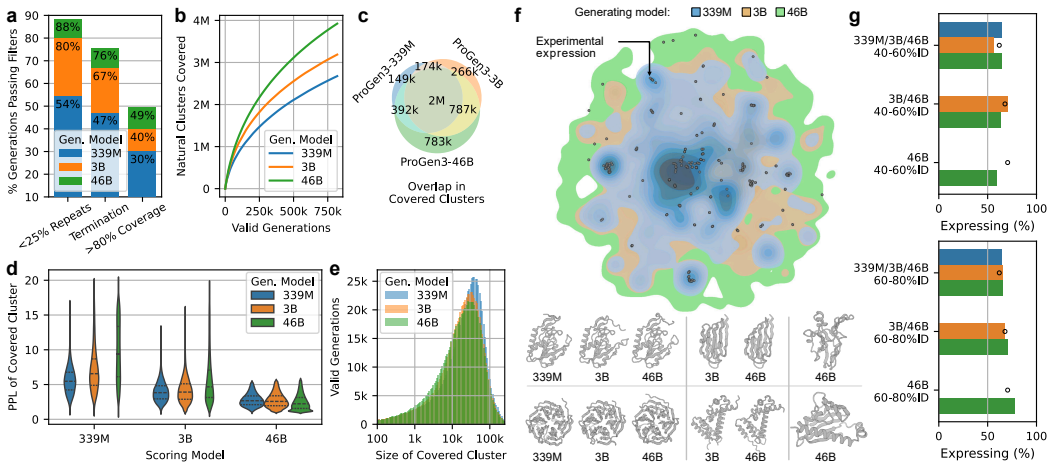

Figure 2: Larger models generate viable proteins for a much more diverse set of families than smaller models. (a) Larger models generate more *valid* sequences that pass a series of quality filters. (b) Valid generations from larger models cover a wider array of naturally occurring 30% ID clusters. (c) The clusters covered by larger models are largely a superset of those covered by smaller models. (d) Larger models generate sequences from clusters whose natural members are assigned high perplexity by smaller models, but not vice versa. (e) Larger models are better able to generate sequences from smaller clusters. (f) Visualization of the clusters selected for experimental characterization, accompanied by ESMFold predicted structures for selected generations. (g) *In vitro* expression rates of model generations for different groups of clusters. Black circles indicate natural protein expression rates for the same clusters.

We now seek to characterize the viability of these generated proteins in the lab. To this end, we perform the split-GFP *E. coli* protein expression assay [11, 12] (Appendix E) to measure soluble protein abundance, which depends on factors including mRNA abundance and stability, translational yield, thermodynamic folding equilibrium, kinetic stability, susceptibility to proteases, aggregation propensity, and toxicity [5, 60]. This assay correlates well with protein expression assayed by direct methods such as SDS-PAGE and Western blotting, is amenable to high throughput assay [61], and has been used to benchmark generative protein models [47].

Given that increased diversity is one of the clearest impacts of scaling up PLMs, we select for experimental characterization 42 clusters that all 3 models generated from, 62 clusters that ProGen3-3B and ProGen3-46B generated from, and 45 clusters that only ProGen3-46B generated from (Figure 2f). From each cluster, we select one sequence per model that is 40-60% ID to a natural sequence in PPA-1, and one sequence that is 60-80% ID. For each (cluster, %ID bucket) pair, the selected sequences have the lowest perplexity according to the model that generated them. We also include as controls two random natural proteins for each cluster, and we ensure that the sequences in the selected clusters span a wide range of lengths (75-300aa) and structural diversity.

Figure 2g reports the cluster-averaged percentage of sequences that showed soluble expression *in vitro*. All models attain similar rates of expression, but larger models do so for a wider range of clusters. As one might expect, generated proteins that are 40-60% ID to a natural tend to have lower rates of expression than those that are 60-80% ID. Interestingly, for all models, the generated proteins expressed at rates similar to random naturals from the clusters they reside in.

3.2 PLMs generate viable proteins outside natural sequence space

Having demonstrated that proteins generated by PLMs residing in sequence clusters alongside naturals are broadly viable, we next turn to sequences for which there is no natural reference point. Specifically, we consider the set of sequences that had less than 30% identity to any protein in PPA-1 (or could not be aligned). From the same set of unconditionally generated sequences, we select 10 generations each that have mostly-alpha, mostly-beta, and mixed alpha/beta secondary structure compositions (as predicted by ESMFold[59]) from ProGen3-339M, ProGen3-3B, and ProGen3-46B, for a total of 90 sequences. First, we consider the rate of expression using the split-GFP assay. We find again that all models are comparable in their ability to generate sequences that express *in vitro*

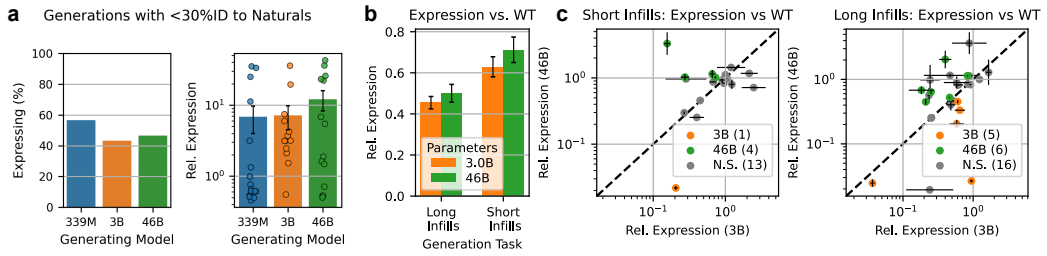

Figure 3: Protein language model generate novel proteins and infill effectively. (a) Expression rates (left) and levels relative to positive control (right) for generated proteins with less than 30% identity to any natural sequence. (b) Expression levels of infilled sequences relative to respective scaffold proteins for long- and short-span infilling tasks. (c) Comparison of relative expression levels for infills generated generated for the same spans by models with 3B and 46B parameters.

(Figure 3a). Next, we considered the expression levels relative to our split-GFP positive control (Figure 3b); here, we see that generations from larger models generally have higher expression.

3.3 Larger PLMs are better infillers

ProGen3's infilling capabilities enable redesigning key segments in the middle of a proteins sequence. To test these capabilities, we selected nine therapeutically or industrially relevant proteins between 100 and 400 AA in length and with some precedence for compatibility with recombinant E. coli expression. For each protein, we used ProGen3-3B and ProGen3-46B to infill sequences for two randomly selected short spans and two randomly selected long spans. We also randomly selected nine additional cytosolic proteins between 100 and 300 AA from the E. coli proteome and used the two models to infill sequences for one short span and one long span. For each infilled span, we experimentally determined the expression levels of two selected sequences from each model, as well as the expression of the corresponding natural protein, using our split-GFP assay.

Eleven of the 18 natural proteins come from the E. coli proteome and may therefore not be expected to express well in our split-GFP assay. While infilled sequences have reduced E. coli expression on average compared to their corresponding natural protein (Figure 3c), there are nonetheless examples of infilled sequences with improved expression over their natural counterpart. Overall, the 46B parameter model slightly outperforms the 3B parameter model, both by the average expression across all infills (Figure 3c) and by the relative expression of infills for the same span. This suggests that larger models may be more adept at understanding the context and constraints present in a given sequence for infilling.

4 Aligning Protein Language Models to Laboratory Data

Zero-shot fitness prediction is often used to evaluate PLMs pre-trained on evolutionary data. Performance is typically measured by the Spearman correlation ρ between model likelihoods and experimentally determined fitness values for the proteins in a deep mutational scan (DMS) dataset [42, 65, 69]. However, due to correlations present in evolutionary dynamics, a PLM's task of faithfully capturing the natural protein distribution can be at odds with zero-shot fitness prediction [103].

Indeed, despite the fact that scaling up model size decreases the validation loss of proteins highly distant from their training data and allows them to generate a much greater diversity of expressing proteins, we find that models larger than 3B parameters often perform worse on the ProteinGym benchmark [69] (Figure 4a). This finding strengthens with more extensive experiments the hypotheses of Weinstein et al. [103] and Gordon et al. [38], that beyond a certain threshold, better estimators of the natural protein distribution can be worse fitness predictors.

Instead, we find that a key advantage of larger models lies in their latent abilities which can be elicited through supervised training. To this end, we use iterative reasoning preference optimization (IRPO, [71]) to align ProGen3 likelihoods with experimentally measured protein properties including activity, binding, organismal fitness, and stability. See Appendix D.1 for more details.

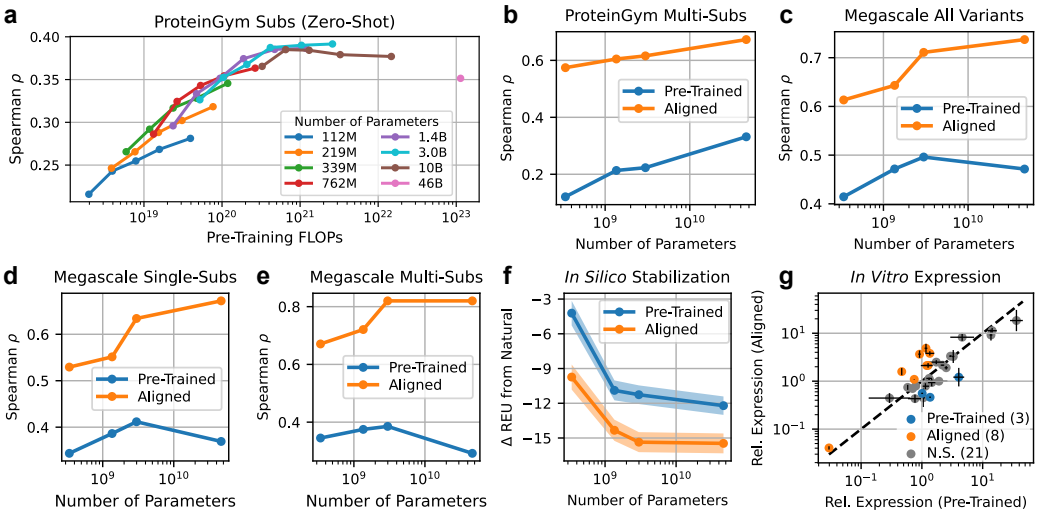

Figure 4: Aligning a model with laboratory data improves its utility for practical design tasks, and larger models are more amenable to alignment. (a) Increasing model scale beyond a certain point degrades zero-shot fitness prediction. (b) Aligning ProGen3 models on a local mutational landscape improves their fitness prediction capabilities for much more distant variants. (c) Aligning ProGen3 models on protein stability datasets allows them to perform out-of-distribution stability prediction. (d) Stability prediction performance on single-substitution variants. (e) Stability prediction performance on multi-substitution variants. (f) Average change in Rosetta energy (REU) between natural proteins and sequences generated using those proteins as prompts. Alignment and model scale both improve the *in silico* stability of generated sequences. (g) Aligning ProGen3-46B on stability data improves the *in vitro* expression of its generations in many cases.

4.1 Supervised Fitness Prediction

First, we demonstrate how alignment can accelerate a directed evolution campaign by training ProGen3 models on a local mutational landscape and performing fitness prediction on more distant variants. We identify all assays in ProteinGym [69] with at least 3 mutations, and we train on all variants at most k mutations from the wild type, where k is the smallest number required for the train split to exceed 500 sequences. To ensure that the train and test splits contain proteins of similar fitness, we require that the total variation distance between the train and test distributions of fitness scores be less than 1. These filters yield 8 assays that measure diverse functional attributes for a wide range of proteins (Supp. Table 8).

With as few as 500 experimental measurements of single-substitution protein variants, aligned models learn generalizable concepts of fitness that allow them to accurately rank proteins that are tens of mutations away from the wild type. The overall fitness prediction performance of aligned models increases with their size (Figure 4b, Supp. Figure 6). An aligned ProGen3-46B ($\rho = 0.673$) outperforms KERMUT [39] ($\rho = 0.628$) and obtains similar performance to ConFit [109] ($\rho = 0.679$). Both baselines are state-of-the-art methods that leverage inductive biases specifically designed to predict the effects of substitutions. In contrast, ProGen3 can also generate novel proteins, and our IRPO formulation can accommodate insertions and deletions as well as substitutions.

Next, we align ProGen3 models with folding free energy measurements (ΔG) from the Megascale protein stability dataset [97], which consists of almost 800,000 single- and double-mutation variants of 479 protein domains. We evaluate how well the models learn a universal concept of stability that generalizes to proteins highly distinct from the training data. Like Widatalla et al. [106], we use FoldSeek `easy-cluster` [98] with 50% alignment coverage to structurally cluster the domains. We hold out 5% of clusters for validation and 5% for testing. Additionally, we only train on single-substitution variants.

As before, increasing model size uniformly improves the stability prediction performance of an aligned model (Figure 4c-e). Using a similar train/val/test split, ProteinDPO [106], a similar method that additionally leverages structural information, obtains comparable overall performance ($\rho = 0.72$) to the aligned ProGen3-46B ($\rho = 0.737$, Figure 4c). However, despite only being trained

on single-substitution variants, our sequence-only method is a much better stability predictor for multi-substitution variants, achieving $\rho = 0.820$ compared to ProteinDPO's $\rho = 0.468$ (Figure 4e).

4.2 Sequence Generation

Encouraged by these results, we now evaluate the generative capabilities of stability-aligned models. From the set tested in Section 3.1, we select as prompts 32 structurally diverse natural proteins that are 98-282 amino acids long (considerably longer than the domains in the Megascale dataset, which are 40-72 amino acids long). We generate 50,000 sequences per model per prompt subject to the quality filters described in Figure 2a, either the C-terminal 75% conditioned on the N-terminal 25%, or the N-terminal 75% conditioned on the C-terminal 25%. For each (model, prompt) combination, we select the 100 sequences passing these quality filters that have the lowest perplexity according to the model that generated them.

As an initial evaluation, we perform an *in silico* characterization of protein stability. For each batch of generated sequences and the corresponding natural sequence prompt, we predict the structure with ESMFold [59] and perform four cycles of minimization (`MinMover`) and relaxation (`FastRelax`) across five independent trajectories in PyRosetta [14]. To evaluate the effects of model scale and alignment on the stability of generated proteins, we calculate the difference in the minimum Rosetta energy achieved for each sequence relative to the corresponding natural (lower is more stable). We find that larger models generally produce more stable proteins and that alignment further stabilizes proteins across model scales (Figure 4f).

Finally, prior work has found that the split-GFP assay correlates positively with protein stability [5, 60]. To determine whether alignment on protein stability data actually improves the stability of generated proteins, we select for each prompt the two lowest-perplexity sequences from both pre-trained and stability-aligned ProGen3-46B models, and we characterize them with the split-GFP assay. In Figure 4g, we plot for each prompt the average expression of each model's generations, normalized by the expression of the wild type protein used to construct each prompt. Using a paired-sample Welch's t-test [104] with $p < 0.01$, we find that alignment improves *in vitro* expression for 8/32 prompts, degrades it for 3/32 prompts, and has no significant effect for 21/32 prompts.

We thus verify both computationally and experimentally that alignment not only improves a ProGen3 model's stability prediction capabilities, but also improves the stability of the sequences it generates. Since alignment also improves out-of-distribution fitness prediction more broadly, we expect that it can be applied to improve models' abilities to generate sequences that optimize a diverse array of functional attributes, and that larger models will see greater gains.

5 Discussion

In this work, we introduce ProGen3, a family of sparse, optimally-scaled generative protein language models (PLMs) trained on one of the largest high-quality protein datasets constructed to date. We systematically demonstrate the importance of curating appropriate data distributions for pre-training PLMs, and we use our findings to train a 46B parameter instantiation of ProGen3 on 1.5T tokens. To our knowledge, ProGen3-46B is the largest sparse PLM yet, and it required 5-10x less compute to pre-train than dense frontier models of a comparable scale [15, 40].

We perform wet lab studies on the relationship between model scale and the fitness of proteins generated by PLMs, and we find that larger models generate viable proteins for a much wider diversity of protein families. Thus, an immediate consequence of model scaling is the ability to better represent rare protein families. Larger models' more general representations also improve their ability to redesign a protein of interest for improved expression, even if that protein is well-represented in the training data. Finally, we show both computationally and experimentally that larger models reap the greatest benefits to their protein fitness prediction and sequence generation capabilities when we align them with laboratory data. In particular, an aligned ProGen3-46B consistently matches or beats state-of-the-art supervised fitness prediction methods while being a far more flexible model.

We have thus demonstrated that larger generative PLMs are more useful tools for a wide range of real-world protein design tasks. Continued model scaling can leverage the exponentially growing amounts of protein sequence data while employing more sophisticated implementations of sparsity to remain highly efficient [29]. However, our results show that ProGen3-46B is already well poised

to advance the vision of designing bespoke proteins for use cases that include drug discovery, enzyme engineering, and industrial processes.

Acknowledgments

We would like to thank Adeline Chen and Rachel Lee for developing our high-throughput lab infrastructure, Eleanor Dunietz for developing our lab informatics systems, and Joseph Gallagher and Peter Cameron for overarching support.

Author Contributions

Data: J.B., S.N.

Pre-Training: A.B., S.J.

Alignment: A.B.

Analysis and Experimental Design: A.B., J.A.R., S.C.C., A.M.H., S.J., A.M.

Split-GFP Experiment: S.C.C., K.C., M.M.

Open Source Development: S.J.

Overall Scientific Direction: A.M., A.B., J.A.R.

Competing Interests

The authors are current or former employees, contractors, or executives of Profluent Bio, Inc. and may hold shares in Profluent Bio, Inc.

Safety and ethics

Computational protein design carries the dual potential to accelerate the development of novel therapeutics and other society-improving molecules, while providing parallel capabilities for nefarious uses, such as engineering of bioweapons. When bolstered by current and future iterations of generative AI, these capabilities are heightened and expected to grow further. The global protein design community has begun to establish appropriate regulations and guidelines towards the continued beneficial development and application of these technologies. We support having a set of community values, guiding principles, and commitments for the responsible development of AI for protein design (https://responsiblebiodesign.ai). Gene synthesis represents a critical step in the actualization of designed protein sequences. The International Gene Synthesis Consortium (IGSC) unites major gene synthesis providers under a commitment to screen all incoming orders against known pathogens and potentially dangerous sequences. As a concrete step towards safe application of protein design technology, all gene synthesis work in support of the present study was performed with IGSC members. For all protein design projects, we urge researchers to maintain ethical oversight throughout project initiation, experimental characterization, and subsequent deployment phases to ensure safety and avoid unintended harmful outcomes. For the set of current models described in this paper for release, we find the benefit of model accessibility to greatly outweigh any theoretical risks.

References

[1] J. Ainslie, J. Lee-Thorp, M. de Jong, Y. Zemlyanskiy, F. Lebron, and S. Sanghai. GQA: Training generalized multi-query transformer models from multi-head checkpoints. In *The 2023 Conference on Empirical Methods in Natural Language Processing*, 2023. URL `https://openreview.net/forum?id=hmOwOZWzYE`.

[2] S. F. Altschul, W. Gish, W. Miller, E. W. Myers, and D. J. Lipman. Basic local alignment search tool. *Journal of Molecular Biology*, 215(3):403–410, 1990. ISSN 0022-2836. doi: https://doi.org/10.1016/S0022-2836(05)80360-2. URL `https://www.sciencedirect.com/science/article/pii/S0022283605803602`.

[3] F. H. Arnold. Design by directed evolution. *Accounts of Chemical Research*, 31(3):125–131, Mar 1998. ISSN 0001-4842. doi: 10.1021/ar960017f. URL https://doi.org/10.1021/ar960017f.

[4] P. Avasthi and R. York. The known protein universe is phylogenetically biased. *Arcadia Science*, Aug 2024. https://research.arcadiascience.com/pub/result-protein-universe-phylogenetic-bias.

[5] D. Balchin, M. Hayer-Hartl, and F. U. Hartl. In vivo aspects of protein folding and quality control. *Science*, 353(6294):aac4354, 2016.

[6] M. Bavarian, H. Jun, N. Tezak, J. Schulman, C. McLeavey, J. Tworek, and M. Chen. Efficient training of language models to fill in the middle, 2022. URL https://arxiv.org/abs/2207.14255.

[7] C. Belliardo, G. D. Koutsovoulos, C. Rancurel, M. Clément, J. Lipuma, M. Bailly-Bechet, and E. G. J. Danchin. Improvement of eukaryotic protein predictions from soil metagenomes. *Scientific Data*, 9(1): 311, Jun 2022. ISSN 2052-4463. doi: 10.1038/s41597-022-01420-4. URL https://doi.org/10.1038/s41597-022-01420-4.

[8] T. Brown, B. Mann, N. Ryder, M. Subbiah, J. D. Kaplan, P. Dhariwal, A. Neelakantan, P. Shyam, G. Sastry, A. Askell, S. Agarwal, A. Herbert-Voss, G. Krueger, T. Henighan, R. Child, A. Ramesh, D. Ziegler, J. Wu, C. Winter, C. Hesse, M. Chen, E. Sigler, M. Litwin, S. Gray, B. Chess, J. Clark, C. Berner, S. McCandlish, A. Radford, I. Sutskever, and D. Amodei. Language models are few-shot learners. In H. Larochelle, M. Ranzato, R. Hadsell, M. Balcan, and H. Lin, editors, *Advances in Neural Information Processing Systems*, volume 33, pages 1877–1901. Curran Associates, Inc., 2020. URL https://proceedings.neurips.cc/paper_files/paper/2020/file/1457c0d6bfcb4967418bfb8ac142f64a-Paper.pdf.

[9] B. Buchfink, K. Reuter, and H.-G. Drost. Sensitive protein alignments at tree-of-life scale using diamond. *Nature Methods*, 18(4):366–368, Apr 2021. ISSN 1548-7105. doi: 10.1038/s41592-021-01101-x. URL https://doi.org/10.1038/s41592-021-01101-x.

[10] B. Bushnell. BBDuk, Mar. 2025. URL sourceforge.net/projects/bbmap/. original-date: 2016-03-08T13:29:36Z.

[11] S. Cabantous and G. S. Waldo. In vivo and in vitro protein solubility assays using split gfp. *Nature methods*, 3(10):845–854, 2006.

[12] S. Cabantous, T. C. Terwilliger, and G. S. Waldo. Protein tagging and detection with engineered self-assembling fragments of green fluorescent protein. *Nature Biotechnology*, 23(1):102–107, Jan 2005. ISSN 1546-1696. doi: 10.1038/nbt1044. URL https://doi.org/10.1038/nbt1044.

[13] A. P. Camargo, S. Roux, F. Schulz, M. Babinski, Y. Xu, B. Hu, P. S. G. Chain, S. Nayfach, and N. C. Kyrpides. Identification of mobile genetic elements with genomad. *Nature Biotechnology*, 42(8):1303–1312, Aug 2024. ISSN 1546-1696. doi: 10.1038/s41587-023-01953-y. URL https://doi.org/10.1038/s41587-023-01953-y.

[14] S. Chaudhury, S. Lyskov, and J. J. Gray. Pyrosetta: a script-based interface for implementing molecular modeling algorithms using rosetta. *Bioinformatics*, 26(5):689–691, 2010.

[15] B. Chen, X. Cheng, P. Li, Y.-a. Geng, J. Gong, S. Li, Z. Bei, X. Tan, B. Wang, X. Zeng, et al. xt-rimopglm: unified 100b-scale pre-trained transformer for deciphering the language of protein. *arXiv preprint arXiv:2401.06199*, 2024.

[16] I.-M. A. Chen, K. Chu, K. Palaniappan, A. Ratner, J. Huang, M. Huntemann, P. Hajek, S. Ritter, N. Varghese, R. Seshadri, S. Roux, T. Woyke, E. A. Eloe-Fadrosh, N. N. Ivanova, and N. C. Kyrpides. The img/m data management and analysis system v.6.0: new tools and advanced capabilities. *Nucleic Acids Research*, 49(D1):D751–D763, Oct 2020. ISSN 0305-1048. doi: 10.1093/nar/gkaa939. URL https://doi.org/10.1093/nar/gkaa939.

[17] S. Chen, C. He, Y. Li, Z. Li, and C. E. Melançon III. A computational toolset for rapid identification of sars-cov-2, other viruses and microorganisms from sequencing data. *Briefings in bioinformatics*, 22(2): 924–935, 2021.

[18] T. Chen, B. Xu, C. Zhang, and C. Guestrin. Training deep nets with sublinear memory cost, 2016. URL https://arxiv.org/abs/1604.06174.

[19] X. Cheng, B. Chen, P. Li, J. Gong, J. Tang, and L. Song. Training compute-optimal protein language models. In A. Globerson, L. Mackey, D. Belgrave, A. Fan, U. Paquet, J. Tomczak, and C. Zhang, editors, *Advances in Neural Information Processing Systems*, volume 37, pages 69386–69418. Curran Associates, Inc., 2024. URL https://proceedings.neurips.cc/paper_files/paper/2024/file/8066ae1446b2bbccb5159587cc3b3bcc-Paper-Conference.pdf.

[20] W.-L. Chiang, L. Zheng, Y. Sheng, A. N. Angelopoulos, T. Li, D. Li, B. Zhu, H. Zhang, M. Jordan, J. E. Gonzalez, and I. Stoica. Chatbot arena: An open platform for evaluating LLMs by human preference. In R. Salakhutdinov, Z. Kolter, K. Heller, A. Weller, N. Oliver, J. Scarlett, and F. Berkenkamp, editors, *Proceedings of the 41st International Conference on Machine Learning*, volume 235 of *Proceedings of Machine Learning Research*, pages 8359–8388. PMLR, 21–27 Jul 2024. URL `https://proceedings.mlr.press/v235/chiang24b.html`.

[21] A. Chowdhery, S. Narang, J. Devlin, M. Bosma, G. Mishra, A. Roberts, P. Barham, H. W. Chung, C. Sutton, S. Gehrmann, P. Schuh, K. Shi, S. Tsvyashchenko, J. Maynez, A. Rao, P. Barnes, Y. Tay, N. Shazeer, V. Prabhakaran, E. Reif, N. Du, B. Hutchinson, R. Pope, J. Bradbury, J. Austin, M. Isard, G. Gur-Ari, P. Yin, T. Duke, A. Levskaya, S. Ghemawat, S. Dev, H. Michalewski, X. Garcia, V. Misra, K. Robinson, L. Fedus, D. Zhou, D. Ippolito, D. Luan, H. Lim, B. Zoph, A. Spiridonov, R. Sepassi, D. Dohan, S. Agrawal, M. Omernick, A. M. Dai, T. S. Pillai, M. Pellat, A. Lewkowycz, E. Moreira, R. Child, O. Polozov, K. Lee, Z. Zhou, X. Wang, B. Saeta, M. Diaz, O. Firat, M. Catasta, J. Wei, K. Meier-Hellstern, D. Eck, J. Dean, S. Petrov, and N. Fiedel. Palm: Scaling language modeling with pathways. *Journal of Machine Learning Research*, 24(240):1–113, 2023. URL `http://jmlr.org/papers/v24/22-1144.html`.

[22] P. F. Christiano, J. Leike, T. Brown, M. Martic, S. Legg, and D. Amodei. Deep reinforcement learning from human preferences. In I. Guyon, U. V. Luxburg, S. Bengio, H. Wallach, R. Fergus, S. Vishwanathan, and R. Garnett, editors, *Advances in Neural Information Processing Systems*, volume 30. Curran Associates, Inc., 2017. URL `https://proceedings.neurips.cc/paper_files/paper/2017/file/d5e2c0adad503c91f91df240d0cd4e49-Paper.pdf`.

[23] K. Cobbe, V. Kosaraju, M. Bavarian, M. Chen, H. Jun, L. Kaiser, M. Plappert, J. Tworek, J. Hilton, R. Nakano, C. Hesse, and J. Schulman. Training verifiers to solve math word problems, 2021. URL `https://arxiv.org/abs/2110.14168`.

[24] A. Cornman, J. West-Roberts, A. P. Camargo, S. Roux, M. Beracochea, M. Mirdita, S. Ovchinnikov, and Y. Hwang. The OMG dataset: An open metagenomic corpus for mixed-modality genomic language modeling. In *The Thirteenth International Conference on Learning Representations*, 2025. URL `https://openreview.net/forum?id=jlzNb1iWs3`.

[25] P. Danecek, J. K. Bonfield, J. Liddle, J. Marshall, V. Ohan, M. O. Pollard, A. Whitwham, T. Keane, S. A. McCarthy, R. M. Davies, et al. Twelve years of samtools and bcftools. *Gigascience*, 10(2):giab008, 2021.

[26] T. Dao. FlashAttention-2: Faster attention with better parallelism and work partitioning. In *International Conference on Learning Representations (ICLR)*, 2024.

[27] J. Dauparas, I. Anishchenko, N. Bennett, H. Bai, R. J. Ragotte, L. F. Milles, B. I. M. Wicky, A. Courbet, R. J. de Haas, N. Bethel, P. J. Y. Leung, T. F. Huddy, S. Pellock, D. Tischer, F. Chan, B. Koepnick, H. Nguyen, A. Kang, B. Sankaran, A. K. Bera, N. P. King, and D. Baker. Robust deep learningbased protein sequence design using proteinmpnn. *Science*, 378(6615):49–56, 2022. doi: 10.1126/science.add2187. URL `https://www.science.org/doi/abs/10.1126/science.add2187`.

[28] Y. N. Dauphin, A. Fan, M. Auli, and D. Grangier. Language modeling with gated convolutional networks. In D. Precup and Y. W. Teh, editors, *Proceedings of the 34th International Conference on Machine Learning*, volume 70 of *Proceedings of Machine Learning Research*, pages 933–941. PMLR, 06–11 Aug 2017. URL `https://proceedings.mlr.press/v70/dauphin17a.html`.

[29] DeepSeek-AI, A. Liu, B. Feng, B. Xue, B. Wang, B. Wu, C. Lu, C. Zhao, C. Deng, C. Zhang, C. Ruan, D. Dai, D. Guo, D. Yang, D. Chen, D. Ji, E. Li, F. Lin, F. Dai, F. Luo, G. Hao, G. Chen, G. Li, H. Zhang, H. Bao, H. Xu, H. Wang, H. Zhang, H. Ding, H. Xin, H. Gao, H. Li, H. Qu, J. L. Cai, J. Liang, J. Guo, J. Ni, J. Li, J. Wang, J. Chen, J. Chen, J. Yuan, J. Qiu, J. Li, J. Song, K. Dong, K. Hu, K. Gao, K. Guan, K. Huang, K. Yu, L. Wang, L. Zhang, L. Xu, L. Xia, L. Zhao, L. Wang, L. Zhang, M. Li, M. Wang, M. Zhang, M. Zhang, M. Tang, M. Li, N. Tian, P. Huang, P. Wang, P. Zhang, Q. Wang, Q. Zhu, Q. Chen, Q. Du, R. J. Chen, R. L. Jin, R. Ge, R. Zhang, R. Pan, R. Wang, R. Xu, R. Zhang, R. Chen, S. S. Li, S. Lu, S. Zhou, S. Chen, S. Wu, S. Ye, S. Ye, S. Ma, S. Wang, S. Zhou, S. Yu, S. Zhou, S. Pan, T. Wang, T. Yun, T. Pei, T. Sun, W. L. Xiao, W. Zeng, W. Zhao, W. An, W. Liu, W. Liang, W. Gao, W. Yu, W. Zhang, X. Q. Li, X. Jin, X. Wang, X. Bi, X. Liu, X. Wang, X. Shen, X. Chen, X. Zhang, X. Chen, X. Nie, X. Sun, X. Wang, X. Cheng, X. Liu, X. Xie, X. Liu, X. Yu, X. Song, X. Shan, X. Zhou, X. Yang, X. Li, X. Su, X. Lin, Y. K. Li, Y. Q. Wang, Y. X. Wei, Y. X. Zhu, Y. Zhang, Y. Xu, Y. Xu, Y. Huang, Y. Li, Y. Zhao, Y. Sun, Y. Li, Y. Wang, Y. Yu, Y. Zheng, Y. Zhang, Y. Shi, Y. Xiong, Y. He, Y. Tang, Y. Piao, Y. Wang, Y. Tan, Y. Ma, Y. Liu, Y. Guo, Y. Wu, Y. Ou, Y. Zhu, Y. Wang, Y. Gong, Y. Zou, Y. He, Y. Zha, Y. Xiong, Y. Ma, Y. Yan, Y. Luo, Y. You, Y. Liu, Y. Zhou, Z. F. Wu, Z. Z. Ren, Z. Ren, Z. Sha, Z. Fu, Z. Xu, Z. Huang, Z. Zhang, Z. Xie, Z. Zhang, Z. Hao, Z. Gou, Z. Ma, Z. Yan, Z. Shao, Z. Xu, Z. Wu, Z. Zhang,

Z. Li, Z. Gu, Z. Zhu, Z. Liu, Z. Li, Z. Xie, Z. Song, Z. Gao, and Z. Pan. Deepseek-v3 technical report, 2024. URL https://arxiv.org/abs/2412.19437.

[30] J. Devlin, M.-W. Chang, K. Lee, and K. Toutanova. BERT: Pre-training of deep bidirectional transformers for language understanding. In J. Burstein, C. Doran, and T. Solorio, editors, *Proceedings of the 2019 Conference of the North American Chapter of the Association for Computational Linguistics: Human Language Technologies, Volume 1 (Long and Short Papers)*, pages 4171–4186, Minneapolis, Minnesota, Jun 2019. Association for Computational Linguistics. doi: 10.18653/v1/N19-1423. URL https://aclanthology.org/N19-1423/.

[31] F. Ding and J. Steinhardt. Protein language models are biased by unequal sequence sampling across the tree of life. *bioRxiv*, 2024. doi: 10.1101/2024.03.07.584001. URL https://www.biorxiv.org/content/early/2024/03/12/2024.03.07.584001.

[32] W. Fedus, B. Zoph, and N. Shazeer. Switch transformers: scaling to trillion parameter models with simple and efficient sparsity. *J. Mach. Learn. Res.*, 23(1), Jan. 2022. ISSN 1532-4435.

[33] Q. Fournier, R. M. Vernon, A. van der Sloot, B. Schulz, S. Chandar, and C. J. Langmead. Protein language models: Is scaling necessary? *bioRxiv*, 2024. doi: 10.1101/2024.09.23.614603. URL https://www.biorxiv.org/content/early/2024/09/23/2024.09.23.614603.

[34] D. M. Fowler and S. Fields. Deep mutational scanning: a new style of protein science. *Nature Methods*, 11(8):801–807, Aug 2014. ISSN 1548-7105. doi: 10.1038/nmeth.3027. URL https://doi.org/10.1038/nmeth.3027.

[35] D. Fried, A. Aghajanyan, J. Lin, S. Wang, E. Wallace, F. Shi, R. Zhong, S. Yih, L. Zettlemoyer, and M. Lewis. Incoder: A generative model for code infilling and synthesis. In *The Eleventh International Conference on Learning Representations*, 2023. URL https://openreview.net/forum?id=hQwb-lbM6EL.

[36] M. C. Frith. A new repeat-masking method enables specific detection of homologous sequences. *Nucleic Acids Research*, 39(4):e23–e23, Nov 2010. ISSN 0305-1048. doi: 10.1093/nar/gkq1212. URL https://doi.org/10.1093/nar/gkq1212.

[37] T. Gale, D. Narayanan, C. Young, and M. Zaharia. Megablocks: Efficient sparse training with mixture-of-experts. In D. Song, M. Carbin, and T. Chen, editors, *Proceedings of Machine Learning and Systems*, volume 5, pages 288–304. Curan, 2023. URL https://proceedings.mlsys.org/paper_files/paper/2023/file/5a54f79333768effe7e8927bcccffe40-Paper-mlsys2023.pdf.

[38] C. W. Gordon, A. X. Lu, and P. Abbeel. Protein language model fitness is a matter of preference. In *The Thirteenth International Conference on Learning Representations*, 2025. URL https://openreview.net/forum?id=UvPdpa4LuV.

[39] P. M. r. Groth, M. Kerrn, L. Olsen, J. Salomon, and W. Boomsma. Kermut: Composite kernel regression for protein variant effects. In A. Globerson, L. Mackey, D. Belgrave, A. Fan, U. Paquet, J. Tomczak, and C. Zhang, editors, *Advances in Neural Information Processing Systems*, volume 37, pages 29514–29565. Curran Associates, Inc., 2024. URL https://proceedings.neurips.cc/paper_files/paper/2024/file/34547650b2ca69d91f3b3c3ae8b21962-Paper-Conference.pdf.

[40] T. Hayes, R. Rao, H. Akin, N. J. Sofroniew, D. Oktay, Z. Lin, R. Verkuil, V. Q. Tran, J. Deaton, M. Wiggert, R. Badkundri, I. Shafkat, J. Gong, A. Derry, R. S. Molina, N. Thomas, Y. A. Khan, C. Mishra, C. Kim, L. J. Bartie, M. Nemeth, P. D. Hsu, T. Sercu, S. Candido, and A. Rives. Simulating 500 million years of evolution with a language model. *Science*, 0(0):eads0018, Jan 2025. doi: 10.1126/science.ads0018. URL https://www.science.org/doi/abs/10.1126/science.ads0018.

[41] D. Hendrycks, C. Burns, S. Basart, A. Zou, M. Mazeika, D. Song, and J. Steinhardt. Measuring massive multitask language understanding. In *International Conference on Learning Representations*, 2021. URL https://openreview.net/forum?id=d7KBjmI3GmQ.

[42] B. L. Hie, K. K. Yang, and P. S. Kim. Evolutionary velocity with protein language models predicts evolutionary dynamics of diverse proteins. *Cell Systems*, 13(4):274–285.e6, 2022. ISSN 2405-4712. doi: https://doi.org/10.1016/j.cels.2022.01.003. URL https://www.sciencedirect.com/science/article/pii/S2405471222000382.

[43] J. Hoffmann, S. Borgeaud, A. Mensch, E. Buchatskaya, T. Cai, E. Rutherford, D. de Las Casas, L. A. Hendricks, J. Welbl, A. Clark, T. Hennigan, E. Noland, K. Millican, G. van den Driessche, B. Damoc, A. Guy, S. Osindero, K. Simonyan, E. Elsen, O. Vinyals, J. W. Rae, and L. Sifre. Training compute-optimal large language models. In *Proceedings of the 36th International Conference on Neural Information Processing Systems*, NeurIPS 2022, Red Hook, NY, USA, 2022. Curran Associates Inc. ISBN 9781713871088.

[44] A. Holtzman, J. Buys, L. Du, M. Forbes, and Y. Choi. The curious case of neural text degeneration. In *International Conference on Learning Representations*, 2020. URL https://openreview.net/forum?id=rygGQyrFvH.

[45] C. Hsu, R. Verkuil, J. Liu, Z. Lin, B. Hie, T. Sercu, A. Lerer, and A. Rives. Learning inverse folding from millions of predicted structures. In K. Chaudhuri, S. Jegelka, L. Song, C. Szepesvari, G. Niu, and S. Sabato, editors, *Proceedings of the 39th International Conference on Machine Learning*, volume 162 of *Proceedings of Machine Learning Research*, pages 8946–8970. PMLR, 17–23 Jul 2022. URL https://proceedings.mlr.press/v162/hsu22a.html.

[46] D. Hyatt, G.-L. Chen, P. F. LoCascio, M. L. Land, F. W. Larimer, and L. J. Hauser. Prodigal: prokaryotic gene recognition and translation initiation site identification. *BMC Bioinformatics*, 11(1):119, Mar 2010. ISSN 1471-2105. doi: 10.1186/1471-2105-11-119. URL https://doi.org/10.1186/1471-2105-11-119.

[47] J. B. Ingraham, M. Baranov, Z. Costello, K. W. Barber, W. Wang, A. Ismail, V. Frappier, D. M. Lord, C. Ng-Thow-Hing, E. R. Van Vlack, S. Tie, V. Xue, S. C. Cowles, A. Leung, J. V. Rodrigues, C. L. Morales-Perez, A. M. Ayoub, R. Green, K. Puentes, F. Oplinger, N. V. Panwar, F. Obermeyer, A. R. Root, A. L. Beam, F. J. Poelwijk, and G. Grigoryan. Illuminating protein space with a programmable generative model. *Nature*, 623(7989):1070–1078, Nov 2023. ISSN 1476-4687. doi: 10.1038/s41586-023-06728-8. URL https://doi.org/10.1038/s41586-023-06728-8.

[48] K. Janocha, A. Ling, A. Godson, Y. Lampi, S. Bornschein, and N. Y. Hammerla. Harnessing preference optimisation in protein lms for hit maturation in cell therapy, 2024. URL https://arxiv.org/abs/2412.01388.

[49] A. Q. Jiang, A. Sablayrolles, A. Roux, A. Mensch, B. Savary, C. Bamford, D. S. Chaplot, D. de las Casas, E. B. Hanna, F. Bressand, G. Lengyel, G. Bour, G. Lample, L. R. Lavaud, L. Saulnier, M.-A. Lachaux, P. Stock, S. Subramanian, S. Yang, S. Antoniak, T. L. Scao, T. Gervet, T. Lavril, T. Wang, T. Lacroix, and W. E. Sayed. Mixtral of experts, 2024. URL https://arxiv.org/abs/2401.04088.

[50] J. Jumper, R. Evans, A. Pritzel, T. Green, M. Figurnov, O. Ronneberger, K. Tunyasuvunakool, R. Bates, A. Žídek, A. Potapenko, A. Bridgland, C. Meyer, S. A. A. Kohl, A. J. Ballard, A. Cowie, B. Romera-Paredes, S. Nikolov, R. Jain, J. Adler, T. Back, S. Petersen, D. Reiman, E. Clancy, M. Zielinski, M. Steinegger, M. Pacholska, T. Berghammer, S. Bodenstein, D. Silver, O. Vinyals, A. W. Senior, K. Kavukcuoglu, P. Kohli, and D. Hassabis. Highly accurate protein structure prediction with alphafold. *Nature*, 596(7873):583–589, Aug 2021. ISSN 1476-4687. doi: 10.1038/s41586-021-03819-2. URL https://doi.org/10.1038/s41586-021-03819-2.

[51] J. Kaplan, S. McCandlish, T. Henighan, T. B. Brown, B. Chess, R. Child, S. Gray, A. Radford, J. Wu, and D. Amodei. Scaling laws for neural language models, 2020. URL https://arxiv.org/abs/2001.08361.

[52] P. J. Keeling, F. Burki, H. M. Wilcox, B. Allam, E. E. Allen, L. A. Amaral-Zettler, E. V. Armbrust, J. M. Archibald, A. K. Bharti, C. J. Bell, B. Beszteri, K. D. Bidle, C. T. Cameron, L. Campbell, D. A. Caron, R. A. Cattolico, J. L. Collier, K. Coyne, S. K. Davy, P. Deschamps, S. T. Dyhrman, B. Edvardsen, R. D. Gates, C. J. Gobler, S. J. Greenwood, S. M. Guida, J. L. Jacobi, K. S. Jakobsen, E. R. James, B. Jenkins, U. John, M. D. Johnson, A. R. Juhl, A. Kamp, L. A. Katz, R. Kiene, A. Kudryavtsev, B. S. Leander, S. Lin, C. Lovejoy, D. Lynn, A. Marchetti, G. McManus, A. M. Nedelcu, S. Menden-Deuer, C. Miceli, T. Mock, M. Montresor, M. A. Moran, S. Murray, G. Nadathur, S. Nagai, P. B. Ngam, B. Palenik, J. Pawlowski, G. Petroni, G. Piganeau, M. C. Posewitz, K. Rengefors, G. Romano, M. E. Rumpho, T. Rynearson, K. B. Schilling, D. C. Schroeder, A. G. B. Simpson, C. H. Slamovits, D. R. Smith, G. J. Smith, S. R. Smith, H. M. Sosik, P. Stief, E. Theriot, S. N. Twary, P. E. Umale, D. Vaulot, B. Wawrik, G. L. Wheeler, W. H. Wilson, Y. Xu, A. Zingone, and A. Z. Worden. The marine microbial eukaryote transcriptome sequencing project (mmetsp): Illuminating the functional diversity of eukaryotic life in the oceans through transcriptome sequencing. *PLOS Biology*, 12(6):1–6, Jun 2014. doi: 10.1371/journal.pbio.1001889. URL https://doi.org/10.1371/journal.pbio.1001889.

[53] D. P. Kingma and J. Ba. Adam: A method for stochastic optimization. In *International Conference on Learning Representations*, 2015. URL https://arxiv.org/abs/1412.6980.

[54] S. Kurtz, A. Phillippy, A. L. Delcher, M. Smoot, M. Shumway, C. Antonescu, and S. L. Salzberg. Versatile and open software for comparing large genomes. *Genome biology*, 5:1–9, 2004.

[55] R. Leinonen, R. Akhtar, E. Birney, L. Bower, A. Cerdeno-Tárraga, Y. Cheng, I. Cleland, N. Faruque, N. Goodgame, R. Gibson, G. Hoad, M. Jang, N. Pakseresht, S. Plaister, R. Radhakrishnan, K. Reddy, S. Sobhany, P. Ten Hoopen, R. Vaughan, V. Zalunin, and G. Cochrane. The european nucleotide archive.

Nucleic Acids Research, 39(D1):D28–D31, Oct 2010. ISSN 0305-1048. doi: 10.1093/nar/gkq967. URL https://doi.org/10.1093/nar/gkq967.

[56] D. Lepikhin, H. Lee, Y. Xu, D. Chen, O. Firat, Y. Huang, M. Krikun, N. Shazeer, and Z. Chen. {GS}hard: Scaling giant models with conditional computation and automatic sharding. In *International Conference on Learning Representations*, 2021. URL https://openreview.net/forum?id=qrwe7XHTmYb.

[57] E. Levy Karin, M. Mirdita, and J. Söding. Metaeuk—sensitive, high-throughput gene discovery, and annotation for large-scale eukaryotic metagenomics. *Microbiome*, 8(1):48, Apr 2020. ISSN 2049-2618. doi: 10.1186/s40168-020-00808-x. URL https://doi.org/10.1186/s40168-020-00808-x.

[58] H. Li. Minimap2: pairwise alignment for nucleotide sequences. *Bioinformatics*, 34(18):3094–3100, 2018.

[59] Z. Lin, H. Akin, R. Rao, B. Hie, Z. Zhu, W. Lu, N. Smetanin, R. Verkuil, O. Kabeli, Y. Shmueli, A. dos Santos Costa, M. Fazel-Zarandi, T. Sercu, S. Candido, and A. Rives. Evolutionary-scale prediction of atomic-level protein structure with a language model. *Science*, 379(6637):1123–1130, 2023. doi: 10.1126/science.ade2574. URL https://www.science.org/doi/abs/10.1126/science.ade2574.

[60] S. Lindman, A. Hernandez-Garcia, O. Szczepankiewicz, B. Frohm, and S. Linse. In vivo protein stabilization based on fragment complementation and a split GFP system. *Proceedings of the National Academy of Sciences*, 107(46):19826–19831, 2010. doi: 10.1073/pnas.1005689107. URL https://www.pnas.org/doi/abs/10.1073/pnas.1005689107.

[61] P. Listwan, T. C. Terwilliger, and G. S. Waldo. Automated, high-throughput platform for protein solubility screening using a split-gfp system. *Journal of structural and functional genomics*, 10:47–55, 2009.

[62] I. Loshchilov and F. Hutter. Decoupled weight decay regularization. In *International Conference on Learning Representations*, 2019. URL https://openreview.net/forum?id=Bkg6RiCqY7.

[63] A. Madani, B. Krause, E. R. Greene, S. Subramanian, B. P. Mohr, J. M. Holton, J. L. Olmos, C. Xiong, Z. Z. Sun, R. Socher, J. S. Fraser, and N. Naik. Large language models generate functional protein sequences across diverse families. *Nature Biotechnology*, 41(8):1099–1106, Aug 2023. ISSN 1546-1696. doi: 10.1038/s41587-022-01618-2. URL https://doi.org/10.1038/s41587-022-01618-2.

[64] G. Marçais and C. Kingsford. A fast, lock-free approach for efficient parallel counting of occurrences of k-mers. *Bioinformatics*, 27(6):764–770, 01 2011. ISSN 1367-4803. doi: 10.1093/bioinformatics/btr011. URL https://doi.org/10.1093/bioinformatics/btr011.

[65] J. Meier, R. Rao, R. Verkuil, J. Liu, T. Sercu, and A. Rives. Language models enable zero-shot prediction of the effects of mutations on protein function. In M. Ranzato, A. Beygelzimer, Y. Dauphin, P. Liang, and J. W. Vaughan, editors, *Advances in Neural Information Processing Systems*, volume 34, pages 29287–29303. Curran Associates, Inc., 2021. URL https://proceedings.neurips.cc/paper_files/paper/2021/file/f51338d736f95dd42427296047067694-Paper.pdf.

[66] P. Micikevicius, S. Narang, J. Alben, G. Diamos, E. Elsen, D. Garcia, B. Ginsburg, M. Houston, O. Kuchaiev, G. Venkatesh, and H. Wu. Mixed precision training. In *International Conference on Learning Representations*, 2018. URL https://openreview.net/forum?id=r1gs9JgRZ.

[67] P. Mistani and V. Mysore. Preference optimization of protein language models as a multi-objective binder design paradigm, 2024. URL https://arxiv.org/abs/2403.04187.

[68] E. Nijkamp, J. A. Ruffolo, E. N. Weinstein, N. Naik, and A. Madani. Progen2: Exploring the boundaries of protein language models. *Cell Systems*, 14(11):968–978.e3, Nov 2023. ISSN 2405-4712. doi: 10.1016/j.cels.2023.10.002. URL https://doi.org/10.1016/j.cels.2023.10.002.

[69] P. Notin, A. Kollasch, D. Ritter, L. van Niekerk, S. Paul, H. Spinner, N. Rollins, A. Shaw, R. Orenbuch, R. Weitzman, J. Frazer, M. Dias, D. Franceschi, Y. Gal, and D. Marks. Proteingym: Large-scale benchmarks for protein fitness prediction and design. In A. Oh, T. Naumann, A. Globerson, K. Saenko, M. Hardt, and S. Levine, editors, *Advances in Neural Information Processing Systems*, volume 36, pages 64331–64379. Curran Associates, Inc., 2023. URL https://proceedings.neurips.cc/paper_files/paper/2023/file/cac723e5ff29f65e3fcbb0739ae91bee-Paper-Datasets_and_Benchmarks.pdf.

[70] P. Notin, R. Weitzman, D. Marks, and Y. Gal. Proteinnpt: Improving protein property prediction and design with non-parametric transformers. In A. Oh, T. Naumann, A. Globerson, K. Saenko, M. Hardt, and S. Levine, editors, *Advances in Neural Information Processing Systems*, volume 36, pages 33529–33563. Curran Associates, Inc., 2023. URL https://proceedings.neurips.cc/paper_files/paper/2023/file/6a4d5d85f7a52f062d23d98d544a5578-Paper-Conference.pdf.

[71] R. Y. Pang, W. Yuan, H. He, K. Cho, S. Sukhbaatar, and J. Weston. Iterative reasoning preference optimization. In A. Globerson, L. Mackey, D. Belgrave, A. Fan, U. Paquet, J. Tomczak, and C. Zhang, editors, *Advances in Neural Information Processing Systems*, volume 37, pages 116617–116637. Curran Associates, Inc., 2024. URL https://proceedings.neurips.cc/paper_files/paper/2024/file/d37c9ad425fe5b65304d500c6edcba00-Paper-Conference.pdf.

[72] A. Paszke, S. Gross, F. Massa, A. Lerer, J. Bradbury, G. Chanan, T. Killeen, Z. Lin, N. Gimelshein, L. Antiga, A. Desmaison, A. Kopf, E. Yang, Z. DeVito, M. Raison, A. Tejani, S. Chilamkurthy, B. Steiner, L. Fang, J. Bai, and S. Chintala. Pytorch: An imperative style, high-performance deep learning library. In H. Wallach, H. Larochelle, A. Beygelzimer, F. d'Alché-Buc, E. Fox, and R. Garnett, editors, *Advances in Neural Information Processing Systems*, volume 32. Curran Associates, Inc., 2019. URL https://proceedings.neurips.cc/paper_files/paper/2019/file/bdbca288fee7f92f2bfa9f7012727740-Paper.pdf.

[73] L. J. Pronk and M. H. Medema. Whokaryote: distinguishing eukaryotic and prokaryotic contigs in metagenomes based on gene structure. *Microbial Genomics*, 8(5):000823, 2022. ISSN 2057-5858. doi: 10.1099/mgen.0.000823. URL https://doi.org/10.1099/mgen.0.000823.

[74] R. Rafailov, A. Sharma, E. Mitchell, C. D. Manning, S. Ermon, and C. Finn. Direct preference optimization: Your language model is secretly a reward model. In *Thirty-seventh Conference on Neural Information Processing Systems*, 2023. URL https://openreview.net/forum?id=HPuSIXJaa9.

[75] C. Raffel, N. Shazeer, A. Roberts, K. Lee, S. Narang, M. Matena, Y. Zhou, W. Li, and P. J. Liu. Exploring the limits of transfer learning with a unified text-to-text transformer. *Journal of Machine Learning Research*, 21(140):1–67, 2020. URL http://jmlr.org/papers/v21/20-074.html.

[76] S. Rajbhandari, J. Rasley, O. Ruwase, and Y. He. Zero: Memory optimizations toward training trillion parameter models, 2020. URL https://arxiv.org/abs/1910.02054.

[77] C. Riquelme, J. Puigcerver, B. Mustafa, M. Neumann, R. Jenatton, A. Susano Pinto, D. Keysers, and N. Houlsby. Scaling vision with sparse mixture of experts. In M. Ranzato, A. Beygelzimer, Y. Dauphin, P. Liang, and J. W. Vaughan, editors, *Advances in Neural Information Processing Systems*, volume 34, pages 8583–8595. Curran Associates, Inc., 2021. URL https://proceedings.neurips.cc/paper_files/paper/2021/file/48237d9f2dea8c74c2a72126cf63d933-Paper.pdf.

[78] A. Rives, J. Meier, T. Sercu, S. Goyal, Z. Lin, J. Liu, D. Guo, M. Ott, C. L. Zitnick, J. Ma, and R. Fergus. Biological structure and function emerge from scaling unsupervised learning to 250 million protein sequences. *PNAS*, 2019. doi: 10.1101/622803. URL https://www.biorxiv.org/content/10.1101/622803v4.

[79] J. A. Ruffolo, A. Bhatnagar, J. Beazer, S. Nayfach, J. Russ, E. Hill, R. Hussain, J. Gallagher, and A. Madani. Adapting protein language models for structure-conditioned design. *bioRxiv*, 2024. doi: 10.1101/2024.08.03.606485. URL https://www.biorxiv.org/content/early/2024/08/03/2024.08.03.606485.

[80] J. A. Ruffolo, S. Nayfach, J. Gallagher, A. Bhatnagar, J. Beazer, R. Hussain, J. Russ, J. Yip, E. Hill, M. Pacesa, A. J. Meeske, P. Cameron, and A. Madani. Design of highly functional genome editors by modeling the universe of crispr-cas sequences. *bioRxiv*, 2024. doi: 10.1101/2024.04.22.590591. URL https://www.biorxiv.org/content/early/2024/04/22/2024.04.22.590591.

[81] E. W. Sayers, E. E. Bolton, J. R. Brister, K. Canese, J. Chan, D. C. Comeau, C. M. Farrell, M. Feldgarden, A. M. Fine, K. Funk, E. Hatcher, S. Kannan, C. Kelly, S. Kim, W. Klimke, M. J. Landrum, S. Lathrop, Z. Lu, T. L. Madden, A. Malheiro, A. Marchler-Bauer, T. D. Murphy, L. Phan, S. Pujar, S. H. Rangwala, V. A. Schneider, T. Tse, J. Wang, J. Ye, B. W. Trawick, K. D. Pruitt, and S. T. Sherry. Database resources of the national center for biotechnology information in 2023. *Nucleic Acids Research*, 51(D1):D29–D38, Nov 2022. ISSN 0305-1048. doi: 10.1093/nar/gkac1032. URL https://doi.org/10.1093/nar/gkac1032.

[82] R. Schmirler, M. Heinzinger, and B. Rost. Fine-tuning protein language models boosts predictions across diverse tasks. *Nature Communications*, 15(1):7407, Aug 2024. ISSN 2041-1723. doi: 10.1038/s41467-024-51844-2. URL https://doi.org/10.1038/s41467-024-51844-2.

[83] D. Sgarbossa, C. Malbranke, and A.-F. Bitbol. Protmamba: a homology-aware but alignment-free protein state space model. *bioRxiv*, 2024. doi: 10.1101/2024.05.24.595730. URL https://www.biorxiv.org/content/early/2024/05/25/2024.05.24.595730.

[84] N. Shazeer. GLU variants improve transformer, 2020. URL https://arxiv.org/abs/2002.05202.

[85] N. Shazeer, A. Mirhoseini, K. Maziarz, A. Davis, Q. Le, G. Hinton, and J. Dean. Outrageously large neural networks: The sparsely-gated mixture-of-experts layer. In *International Conference on Learning Representations*, 2017. URL https://openreview.net/forum?id=B1ckMDqlg.

[86] R. W. Shuai, J. A. Ruffolo, and J. J. Gray. Iglm: Infilling language modeling for antibody sequence design. *Cell Systems*, 14(11):979–989, 2023.

[87] M. Steinegger, M. Mirdita, and J. Söding. Protein-level assembly increases protein sequence recovery from metagenomic samples manyfold. *Nature Methods*, 16(7):603–606, Jul 2019. ISSN 1548-7105. doi: 10.1038/s41592-019-0437-4. URL https://doi.org/10.1038/s41592-019-0437-4.

[88] F. Stocco, M. Artigues-Lleixa, A. Hunklinger, T. Widatalla, M. Guell, and N. Ferruz. Guiding generative protein language models with reinforcement learning, 2025. URL https://arxiv.org/abs/2412.12979.

[89] J. Su, M. Ahmed, Y. Lu, S. Pan, W. Bo, and Y. Liu. Roformer: Enhanced transformer with rotary position embedding. *Neurocomputing*, 568(C), Feb 2024. ISSN 0925-2312. doi: 10.1016/j.neucom.2023.127063. URL https://doi.org/10.1016/j.neucom.2023.127063.

[90] N. Sun, S. Zou, T. Tao, S. Mahbub, D. Li, Y. Zhuang, H. Wang, X. Cheng, L. Song, and E. P. Xing. Mixture of experts enable efficient and effective protein understanding and design. *bioRxiv*, 2024. doi: 10.1101/2024.11.29.625425. URL https://www.biorxiv.org/content/early/2024/12/03/2024.11.29.625425.

[91] B. E. Suzek, H. Huang, P. McGarvey, R. Mazumder, and C. H. Wu. Uniref: comprehensive and non-redundant uniprot reference clusters. *Bioinformatics*, 23(10):1282–1288, Mar 2007. ISSN 1367-4803. doi: 10.1093/bioinformatics/btm098. URL https://doi.org/10.1093/bioinformatics/btm098.

[92] Y. Tay, M. Dehghani, V. Q. Tran, X. Garcia, J. Wei, X. Wang, H. W. Chung, D. Bahri, T. Schuster, S. Zheng, D. Zhou, N. Houlsby, and D. Metzler. UL2: Unifying language learning paradigms. In *The Eleventh International Conference on Learning Representations*, 2023. URL https://openreview.net/forum?id=6ruVLB727MC.

[93] The Mosaic ML Team. composer. https://github.com/mosaicml/composer/, 2021.

[94] The Mosaic ML Team. streaming. https://github.com/mosaicml/streaming/, 2022.

[95] H. Touvron, T. Lavril, G. Izacard, X. Martinet, M.-A. Lachaux, T. Lacroix, B. Rozière, N. Goyal, E. Hambro, F. Azhar, A. Rodriguez, A. Joulin, E. Grave, and G. Lample. Llama: Open and efficient foundation language models, 2023. URL https://arxiv.org/abs/2302.13971.

[96] T. Truong Jr and T. Bepler. Poet: A generative model of protein families as sequences-of-sequences. In A. Oh, T. Naumann, A. Globerson, K. Saenko, M. Hardt, and S. Levine, editors, *Advances in Neural Information Processing Systems*, volume 36, pages 77379–77415. Curran Associates, Inc., 2023. URL https://proceedings.neurips.cc/paper_files/paper/2023/file/f4366126eba252699b280e8f93c0ab2f-Paper-Conference.pdf.

[97] K. Tsuboyama, J. Dauparas, J. Chen, E. Laine, Y. Mohseni Behbahani, J. J. Weinstein, N. M. Mangan, S. Ovchinnikov, and G. J. Rocklin. Mega-scale experimental analysis of protein folding stability in biology and design. *Nature*, 620(7973):434–444, Aug 2023. ISSN 1476-4687. doi: 10.1038/s41586-023-06328-6. URL https://doi.org/10.1038/s41586-023-06328-6.

[98] M. van Kempen, S. S. Kim, C. Tumescheit, M. Mirdita, J. Lee, C. L. M. Gilchrist, J. Söding, and M. Steinegger. Fast and accurate protein structure search with foldseek. *Nature Biotechnology*, 42(2):243–246, Feb 2024. ISSN 1546-1696. doi: 10.1038/s41587-023-01773-0. URL https://doi.org/10.1038/s41587-023-01773-0.

[99] A. Vaswani, N. Shazeer, N. Parmar, J. Uszkoreit, L. Jones, A. N. Gomez, L. u. Kaiser, and I. Polosukhin. Attention is all you need. In I. Guyon, U. V. Luxburg, S. Bengio, H. Wallach, R. Fergus, S. Vishwanathan, and R. Garnett, editors, *Advances in Neural Information Processing Systems*, volume 30. Curran Associates, Inc., 2017. URL https://proceedings.neurips.cc/paper_files/paper/2017/file/3f5ee243547dee91fbd053c1c4a845aa-Paper.pdf.

[100] A. Wang, Y. Pruksachatkun, N. Nangia, A. Singh, J. Michael, F. Hill, O. Levy, and S. Bowman. Superglue: A stickier benchmark for general-purpose language understanding systems. In H. Wallach, H. Larochelle, A. Beygelzimer, F. d'Alché-Buc, E. Fox, and R. Garnett, editors, *Advances in Neural Information Processing Systems*, volume 32. Curran Associates, Inc., 2019. URL https://proceedings.neurips.cc/paper_files/paper/2019/file/4496bf24afe7fab6f046bf4923da8de6-Paper.pdf.

[101] A. Wang, A. Singh, J. Michael, F. Hill, O. Levy, and S. R. Bowman. GLUE: A multi-task benchmark and analysis platform for natural language understanding. In *International Conference on Learning Representations*, 2019. URL https://openreview.net/forum?id=rJ4km2R5t7.

[102] J. Wei, M. Bosma, V. Zhao, K. Guu, A. W. Yu, B. Lester, N. Du, A. M. Dai, and Q. V. Le. Finetuned language models are zero-shot learners. In *International Conference on Learning Representations*, 2022. URL https://openreview.net/forum?id=gEZrGCozdqR.

[103] E. N. Weinstein, A. N. Amin, J. Frazer, and D. S. Marks. Non-identifiability and the blessings of misspecification in models of molecular fitness. In A. H. Oh, A. Agarwal, D. Belgrave, and K. Cho, editors, *Advances in Neural Information Processing Systems*, 2022. URL https://openreview.net/forum?id=CwG-o0ind6t.

[104] B. L. Welch. The generalization of 'student's' problem when several different population variances are involved. *Biometrika*, 34(1-2):28–35, Jan 1947. doi: 10.2307/2332510.

[105] S. Welleck, I. Kulikov, S. Roller, E. Dinan, K. Cho, and J. Weston. Neural text generation with unlikelihood training. In *International Conference on Learning Representations*, 2020. URL https://openreview.net/forum?id=SJeYe0NtvH.

[106] T. Widatalla, R. Rafailov, and B. Hie. Aligning protein generative models with experimental fitness via direct preference optimization. *bioRxiv*, 2024. doi: 10.1101/2024.05.20.595026. URL https://www.biorxiv.org/content/early/2024/05/21/2024.05.20.595026.

[107] R. Xiong, Y. Yang, D. He, K. Zheng, S. Zheng, C. Xing, H. Zhang, Y. Lan, L. Wang, and T. Liu. On layer normalization in the transformer architecture. In H. D. III and A. Singh, editors, *Proceedings of the 37th International Conference on Machine Learning*, volume 119 of *Proceedings of Machine Learning Research*, pages 10524–10533. PMLR, 13–18 Jul 2020. URL https://proceedings.mlr.press/v119/xiong20b.html.

[108] B. Zhang and R. Sennrich. Root mean square layer normalization. In H. Wallach, H. Larochelle, A. Beygelzimer, F. d'Alché-Buc, E. Fox, and R. Garnett, editors, *Advances in Neural Information Processing Systems*, volume 32. Curran Associates, Inc., 2019. URL https://proceedings.neurips.cc/paper_files/paper/2019/file/1e8a19426224ca89e83cef47f1e7f53b-Paper.pdf.

[109] J. Zhao, C. Zhang, and Y. Luo. Contrastive fitness learning: Reprogramming protein language models for low-n learning of protein fitness landscape. In J. Ma, editor, *Research in Computational Molecular Biology*, pages 470–474, Cham, 2024. Springer Nature Switzerland. ISBN 978-1-0716-3989-4.

[110] D. M. Ziegler, N. Stiennon, J. Wu, T. B. Brown, A. Radford, D. Amodei, P. Christiano, and G. Irving. Fine-tuning language models from human preferences, 2020. URL https://arxiv.org/abs/1909.08593.

[111] V. Zulkower and S. Rosser. DNA Chisel, a versatile sequence optimizer. *Bioinformatics*, 36(16):4508–4509, 2020.

A Related Work

A.1 Mixture of Experts

Scaling up model size is one of the most important ways to improve the performance of deep learning models [43, 51]. However, larger models are also more compute-intensive. Mixture of Experts (MoE) layers leverage sparsity to increase model efficiency [85]. These layers consist of multiple expert sub-networks, and they route each individual token to a different subset of experts. Transformer models trained in NLP [29, 32, 49, 56], computer vision [77], and PLM [90] domain have replaced the feedforward network with a MoE to unlock significant speedups while maintaining performance comparable to a dense model.

A.2 Protein Language Models

Protein language models (PLMs) encompass a wide range of approaches including causal decoders that generate novel proteins from scratch [63, 68, 80] or infill spans in the middle of a protein [15, 86], bidirectional encoders useful for protein understanding [40, 59, 78, 90], and inverse folding models that generate proteins conditioned on a user-specified structure [27, 45, 79], among others. These models are typically pre-trained on large databases of naturally occurring proteins. Compute-optimal scaling laws have been derived for dense PLMs [19], but it is unclear whether they also apply to sparse PLMs.

Limited work has been done to determine the best data distributions for training PLMs, and prior works have largely relied on a range of ad-hoc distributions. Lin et al. [59] and Hayes et al. [40] de-replicated their data at 90% ID and respectively sampled each 50% and 70% ID cluster with equal probability. Nijkamp et al. [68] and Cheng et al. [19] de-replicated their genomic data at 90% ID and their metagenomic data at 30% ID. Chen et al. [15] and Sun et al. [90] de-replicated their genomic data at 90% ID and included at most 10 sequences per 30% ID cluster for their metagenomic data. Meanwhile, Fournier et al. [33] found the best results without any resampling.

A.3 Model Alignment

As language models grow, they acquire increasingly useful emergent properties over the course of unsupervised training [8, 21, 49, 59, 68, 95]. However, out of the box, they are often ill-suited to tasks that their users care about, from generating performant code to designing more stable proteins. Alignment algorithms leverage supervised data to direct language model generations to match a user's preferences. These include fine-tuning on a curated set of positive examples [68, 82, 102], reinforcement learning to maximize the user-specified rewards achieved by a language model's conditional generations [22, 110], and direct alignment algorithms that reformulate the reinforcement learning task as an easier supervised learning task [71, 74]. For PLMs, direct alignment algorithms have improved models for inverse folding [40, 106], fitness prediction [109], function-guided generation [40, 88], and binder design [48, 67].

B Profluent Protein Atlas

To train ProGen3, we curated the Profluent Protein Atlas v1 (PPA-1). Table 1 summarizes the composition of the dataset. We collected genomic and metagenomic datasets from IMG/M [16], ENA [55], and NCBI GenBank [81], and we performed protein coding prediction using `prodigal-gv` [13, 46]. We discarded contigs shorter than 1,000 bp as well as contigs with coding density <65% to remove mispredicted proteins from eukaryotic sequences [73]. These were combined with proteins from UniRef [91], NCBI NR [81], and five additional metagenome and eukaryotic-focused databases, resulting in a total of 12.2B proteins. All proteins were subject to additional filters to remove proteins with >8000 amino acids, protein fragments, and proteins with invalid amino acids, k-mer repeats [80], or >50% low complexity regions [36]. This resulted in a final filtered set of 3.4B proteins.

On this filtered set, we performed hierarchical clustering at 90%, 50%, and 30% amino acid identity using DIAMOND [9]. At each clustering step, we used the representative sequences from the previous round (e.g., 50% identity clustering was performed on the 90% identity cluster representatives).

Clustering at each level was conducted iteratively across four sensitivity settings, where the representatives from one setting were clustered further at the next. The number of sensitivity levels varied by identity threshold: at 90% identity, we applied only `--linclust`, while at 50% and 30% identity, we used `--linclust`, `--fast`, `--default`, and `--more-sensitive`. This pipeline yielded 1.2B 90% ID clusters, 183M 50% ID clusters, and 113M 30% ID clusters.

We compare PPA-1 to other protein datasets in Table 2. After filtering and clustering, PPA-1 is of similar scale and diversity to the OMG dataset [24]. It is of similar scale to the dataset used to train ESM3 [40], but it does not include any protein fragments while ESM3's dataset does. It is also considerably larger than resources like UniRef [91] and BFD [50, 87].

Data Source	Type	Proteins (Total)	Proteins (Filtered)	Percentage
IMG/M [16]	Metagenomic	5,313,407,975	1,402,061,253	41.28%
ENA [55]	Metagenomic	3,324,676,018	946,087,610	27.85%
NCBI-nr [81]	Genomic	542,683,057	471,482,093	13.88%
GenBank [81]	Genomic	455,377,658	362,034,076	10.66%
UniRef90 [91]	Genomic	170,669,877	144,914,015	4.27%
SRC [87]	Metagenomic	2,020,821,851	60,061,204	1.77%
MMETSP [52]	Metagenomic	28,029,947	3,837,925	0.11%
SoilEuk [7]	Metagenomic	5,366,252	3,450,399	0.10%
MERC [87]	Metagenomic	291,261,719	1,994,696	0.06%
MetaEuk [57]	Metagenomic	6,310,729	258,456	0.01%
Total	—	12,158,605,083	3,396,181,727	100%

Table 1: Composition of the Profluent Protein Atlas.

Dataset	Fragments Removed	30% ID clusters	50% ID Clusters	Proteins
UniRef [91]	✗	—	69M	454M
BFD [50, 87]	✗	66M	—	2204M
ESM3 [40]	✗	—	—	3143M
OMG [24]	✓	—	207M	3300M
PPA-1 (ours)	✓	113M	183M	3396M

Table 2: Comparison of the Profluent Protein Atlas to other large protein datasets.

C Pre-Training

C.1 Implementation and Hyperparameters

All ProGen3 models are transformer based decoder-only models[99] with a context length of 8192 tokens and Transformer++ optimizations [95]: feedforward networks with SwiGLU activations [28, 84], rotary positional embeddings (RoPE [89]), grouped query attention [1], and pre-layer normalization [107] using RMSNorm [108]. For RoPE, we use $\theta = 10^5$. Unless otherwise specified, we replace all feed-forward layers with a Mixture of Experts (MoE) that activates 2 experts (out of 8 total) for each token [32, 85]:

$$\mathrm{MoE}(x) = \sum_{i=1}^{8} \mathrm{Softmax}(\mathrm{Top2}(W_g x))_i \cdot \mathrm{FFN}_i(x), \tag{2}$$

where $x \in \mathbb{R}^d$ is a single token embedding, $W_g \in \mathbb{R}^{8\times d}$ is a linear routing layer, and $\mathrm{FFN}_i : \mathbb{R}^d \to \mathbb{R}^d$ is an expert sub-network. We regularize our language modeling loss with the load balancing loss used by SwitchTransformer [32] multiplied by a weight $\lambda = 0.05$.

All models are trained using the AdamW optimizer [53, 62] with $\beta_1 = 0.9$, $\beta_2 = 0.95$, and BF16 mixed precision [66]. After an initial warmup period, we decay the learning rate to 10% of its peak value following a cosine schedule. We leverage fully sharded data parallel training [76] and gradient checkpointing [18] for memory-efficient distributed training.

We implement our models using PyTorch [72]. To improve efficiency, we use `FlashAttention2` [26] and `Megablocks` [37] for our attention and MoE layers, respectively. Finally, we orchestrate training and data loading with MosaicML's `composer` [93] and `streaming` [94] libraries, respectively.

Table 3 describes our model configurations and pre-training hyperparameters in more detail.

Params (Active)	Layers	d_{model}	Attn Heads	d_{FFN}	LR	WD	BSZ	WU
112M (32M)	10	384	6	1152	5e-4	5e-6	1M	2000
219M (63M)	11	512	8	1536	5e-4	5e-6	1M	2000
339M (98M)	17	512	8	1536	5e-4	5e-6	1M	2000
762M (221M)	17	768	12	2304	5e-4	5e-6	1M	2000
1.4B (393M)	17	1024	16	3072	5e-4	5e-6	1M	2000
3.0B (866M)	24	1280	16	3840	5e-4	5e-6	1M	2000
10B (2.7B)	24	2048	16 (8 KV)	8192	5e-4	5e-6	2M	2000
46B (12.6B)	32	4096	32 (8 KV)	14336	3.2e-4	4e-6	3M	10000

Table 3: Model configurations and pre-training hyperparameters. BSZ is the number of tokens per batch. WU is the number of warmup steps and is kept constant regardless of total training duration.

C.2 Mixture of Experts Performance

To validate the performance of sparse architectures, we train three models for 80B tokens: a dense 1.4B parameter model, a sparse 1.4B parameter model, and a sparse 3B parameter model. In Table 4, we find that the dense 1.4B parameter model slightly outperforms the sparse 1.4B parameter model. However, the sparse 3B parameter model significantly outperforms both while requiring about half the FLOPs of the smaller dense model.

Architecture	Parameters	Active Parameters	FLOPs	Validation Loss
Dense	1,386,084,352	1,386,084,352	1.10×10^{20}	1.920
Sparse	1,355,871,232	393,174,016	3.14×10^{19}	1.948
Sparse	2,989,920,000	866,369,280	6.93×10^{19}	1.849

Table 4: Validation loss of dense and sparse architectures trained for 80B tokens. For a fixed number of parameters, dense models slightly outperform sparse ones. For a fixed FLOPs budget, sparse models outperform dense ones.

C.3 Training Tasks

Training Protein Language Models with a standard autoregressive modeling objective supports generating protein sequences from the N-to-C terminal or C-to-N terminal, conditioned on the previous residues in the sequence [63, 68]. This formulation precludes settings where we only want to generate a segment in the middle of the protein while keeping both prior and subsequent amino acids fixed. To support this, we augment the ProGen3 model training with an infilling or *generalized language modeling (GLM)* learning objective, taking inspiration from multiple prior works in NLP [6, 35, 75, 92] and Protein Language Modeling [15, 83].

Infilling Training Details During ProGen3 training, we used the infilling objective for 1/3 of the sequences seen by the model (i.e., the GLM to CLM ratio is 1:2). For each such case, we sample N spans from the sequence, up until a maximum length fraction f. The span length of each span is sampled from a truncated mixture of Gaussians, where we assign equal probability to each of $\mathcal{N}(10, 5)$, $\mathcal{N}(30, 10)$, $\mathcal{N}(70, 20)$, $\mathcal{N}(200, 50)$, and $\mathcal{N}(400, 100)$, denoted as $\mathcal{N}(\mu, \sigma)$. The maximum length fraction f is itself sampled from the set $\{0.15, 0.25, 0.5, 0.8\}$ with probabilities $\{0.28, 0.3, 0.28, 0.14\}$ respectively.

For each span, we sample the start position uniformly from the protein sequence and we replace the corresponding span of residues (span start, span start + span length) with a single sentinel token `<span_i>`. At the same time, the same sentinel token is appended to the end of the sequence,

	Validation PPL (Distinct @50%)			
Hyperparameter	CLM	GLM ($L = 10$)	GLM ($L = 50$)	GLM ($L = 200$)
Infilling to CLM Ratio				
0	8.40	–	–	–
1:10	8.82	20.86	>100	>100
1:4	8.98	14.84	>100	>100
1:2	9.13	**12.05**	>100	>100
1:1	9.41	12.47	>100	>100
Mask Fractions and Span Lengths				
$L \leq 10, f \leq 0.15$	9.13	12.05	>100	>100
$L \leq 30, f \leq 0.25$	9.08	9.64	49.16	>100
$L \leq 70, f \leq 0.50$	9.09	9.71	9.68	9.44
$L \leq 200, f \leq 0.50$	**9.02**	**9.54**	**9.34**	**8.91**
Positional Encoding Strategy				
Naive	8.98	9.47	9.30	8.87
Position-Preserving	8.99	9.08	**8.86**	8.56
Fuzzy Position-Preserving	**8.90**	**8.30**	8.87	**8.56**

Table 5: Validation Loss on CLM and Single Span Infilling Tasks for various infilling setup ablations.

followed by the residues in the span being replaced and finally an end of span token. The constructed sequence is then used to train the model with a causal attention mask and autoregressive modeling loss over the whole sequence. Similar to ProGen2 [68], we use a `1` token to denote the N-terminal and a `2` token to denote the C-terminal, enabling us to perform both CLM and GLM tasks in the N-to-C or C-to-N direction.

Position Preserving Fuzzy Encoding When the infilled residues are transposed to the end of the sequence, they retain their original position ids, and the sentinel span tokens get the same position id as the first token of the infilled span. A drawback of this scheme is that the model will have a strong bias towards exactly the same number of residues that have been removed from the prefix. To mitigate this and allow the model to stop early, for each infilled span, we add a fuzzy length factor to the position ids of all tokens that come after that span. The fuzzy factor is sampled from a geometric distribution with a mean of 0.2 times the length of the span. We provide an example below with infilled spans highlighted in color.

```
Original Sequence: ASVGFKAGVKDYKLTYYTPEYETLDTD
------------------------------------------------------------------------------
Infilling Sequence: <bos_glm> 1 A S V G F <span_38> K D Y K L T Y Y T
   Position Ids :        0      1 2 3 4 5 6      7      12 13 14 15 16 17 18 19 20
<span_6> L D T D 2 <eos> <span_38> K A G V <eos_span> <span_6> P E
   21    29 30 31 32 33   34        7     8 9 10 11      12         21     22 23
Y E T <eos_span>
24 25 26      27
```

Ablations We validated various design decisions described in the previous paragraphs using validation perplexity, measured on the sequences from the held-out clusters distinct at 50% from the training set for both CLM task (to measure any degradation in CLM performance) and single span infilling. For the latter, we remove a random span of length L from each validation example and measure the perplexity of the suffix after the infilling transformation as described previously (i.e. perplexity of tokens after the `<eos>` token). The results from these ablations can be found in Table 5. Initially, we only infilled spans up to length 10 for infilling and varied the proportion of infilling examples seen during training. We observed that CLM performance shows small degradation (with 1pt perplexity difference) as we vary the proportion from 0 to 1:1, while infilling perplexity varies significantly. We selected a ratio of 1:2 as a compromise. In addition, we also observed that this set of models had very high perplexity for infilling spans of length 50 and 200. Therefore, in the next set of experiments, we vary the length of spans and the mask fraction seen by the model. We see that increasing lengths and mask fraction generally improve performance across all validation sets,

validating our choice of using a mixture of Gaussians with mean lengths of up to 400. Finally, we observed that using position-preserving position encoding improved perplexities, while fuzzy length encoding did not lead to any significant performance degradation. Hence, we adopted both of these enhancements.

C.4 Importance of Warmup Duration

In Section 2.3, we found that the 46B parameter model achieved a validation loss lower than the compute-optimal frontier our scaling laws predicted. A key difference between this model and the smaller ones is that we increased its warmup from 2,000 steps to 10,000 steps to stabilize training (Table 3). This discrepancy could explain the gap in performance, as we find that using 8,000 steps of warmup instead of 2,000 steps improves the final training and validation loss of a 1.4B parameter model trained for 80B tokens (80,000 steps) (Figure 5).

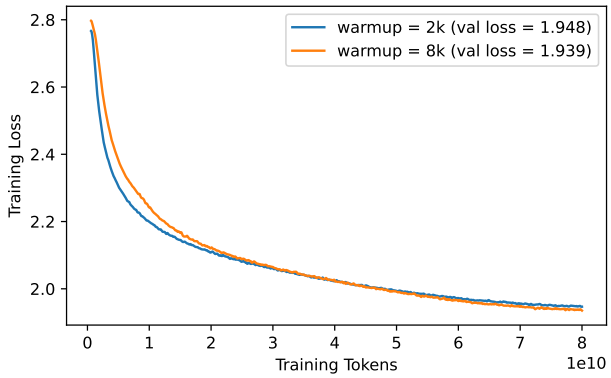

Figure 5: Increasing warmup from 2000 steps to 8000 steps improves the final training and validation loss for a 1.4B parameter model trained on 80B tokens.

D Model Alignment

D.1 Implementation and Hyperparameters

The most relevant alignment algorithms for this paper are direct preference optimization (DPO, [74]) and its generalization iterative reasoning preference optimization (IRPO, [71]). Let p_θ be the model we are aligning, p_{ref} be the pre-trained model, $\mathcal{D}$ be our alignment dataset, x be conditioning information, $y \mid x$ be a completion, and R be the reward assigned to $y \mid x$. IRPO can be formulated as

$$\min_\theta \mathop{\mathbb{E}}_{x,((y_1,R_1),\ldots,(y_n,R_n))\sim\mathcal{D}} \sum_{R_i>R_j} -\log\sigma\left(\beta\log\frac{p_\theta(y_i \mid x)}{p_{\text{ref}}(y_i \mid x)} - \beta\log\frac{p_\theta(y_j \mid x)}{p_{\text{ref}}(y_j \mid x)}\right) + \alpha \sum_{R_i=\max R_1,\ldots,R_n} -\frac{\log p_\theta(y_i \mid x)}{|y_i|}. \tag{3}$$

The first term encourages the aligned model p_θ to assign higher likelihood to preferred completions than dispreferred ones. β controls the amount we allow the aligned model p_θ to deviate from the pre-trained model p_{ref}; larger values allow less deviation. The richness of this loss also increases with the *block size* n, i.e. the number of completions that are directly comparable with each other. The second term is the negative log likelihood loss of the completions with the highest reward. If we set the regularization strength $\alpha = 0$, IRPO reduces to DPO.

In this paper, we let the conditioning information x denote a single DMS assay, y_i denote a protein characterized in that assay, and R_i its experimentally measured fitness (ΔG for the Megascale dataset). We use a cosine learning rate schedule that decays to 50% of the peak learning rate over training and uses the first 10% of steps for a linear warmup. We train all models with peak learning rate 3×10^{-6} and peak weight decay 3×10^{-8}.

Parameters	Pre-Train Tokens	β	α	# Epochs (ProteinGym)	# Epochs (Megascale)
339M	200B	0.10	0.05	25	6
1.4B	500B	0.10	0.05	25	6
3B	500B	0.10	0.02	25	6
46B	1.5T	0.10	0.01	25	10

Table 6: Training hyperparameters for IRPO.

Model	α	Block Size	Spearman ρ	Validation Perplexity
1.4B (Pre-Trained)	–	–	0.471	8.150
1.4B	0.05	8	0.562	9.384
1.4B	0.05	16	0.639	9.607
1.4B	0.05	64	0.643	9.712
1.4B (DPO)	0	64	0.670	13.874
1.4B	0.02	64	0.650	10.551
1.4B	0.05	64	0.643	9.712
1.4B	0.1	64	0.629	9.241

Table 7: Larger block sizes improve fitness prediction performance. Increasing the IRPO regularization coefficient α improves validation perplexity at the cost of fitness prediction performance.

For the ProteinGym experiments, we train a separate set of models for each assay in Table 8. We use a common set of hyperparameters across all configurations; the only exception is that we decrease the batch size from 64 to 32 if the training dataset contains fewer than 1000 samples. Since we are only training on a single assay, the block size n is the same as the batch size.

For all Megascale experiments, we a single model on the entire training set with a batch size of 1024 and block size n of 64. We select the training duration via early stopping on the validation Spearman ρ. Table 6 reports additional training hyperparameters that vary between models.

D.2 IRPO Ablation Studies

We select the α hyperparameter and block size n for each model by training on the Megascale protein stability dataset and evaluating fitness prediction performance on the Megascale validation set, as well as the model's perplexity on the validation set used for pre-training.

Table 7 shows representative trends for a 1.4B parameter model. In general, increasing the block size n improves fitness prediction performance with minimal impact to validation perplexity. This makes sense because the number of comparisons in Equation 3 scales quadratically with n, so increasing n imbues the loss with much richer information about the overall fitness landscape. For this reason, we proceed with a fairly large block size of 64 wherever possible.

We also find that the NLL loss term of IRPO is an important regularizer that prevents the validation perplexity from degrading too much, i.e. it allows aligned models to retain the broad knowledge about proteins that they gained during pre-training. For each model size, we select the value of α which achieves the best fitness prediction performance while obtaining a validation perplexity no more than 2 points higher than the pre-trained model's. This process yields the values described in Table 6.

D.3 ProteinGym Alignment Experiments

In Figure 6, we report the fitness prediction performance of both pre-trained and aligned models on each of the 8 assays described in Table 8. Figure 4b in the main text reports the average Spearman ρ across these assays. Across the board, aligned models outperform their zero-shot counterparts.

For the five assays with at least 500 single-mutation variants (i.e. the ones where we trained only on single-mutation variants), the performance of the aligned models improves monotonically with their scale. KERMUT and ConFit obtain similar performance to ProGen3-46B on the 4 activity assays;

Dataset ID	Coarse Selection Type	Max # Mutations (Train)	# Train Variants	Max # Mutations (Test)	# Test Variants
D7PM05_CLYGR_Somermeyer_2022	Activity	1	1169	23	23,346
GFP_AEQVI_Sarkisyan_2016	Activity	1	1084	15	50,630
Q6WV12_9MAXI_Somermeyer_2022	Activity	1	1141	13	30,260
Q8WTC7_9CNID_Somermeyer_2022	Activity	1	1201	43	32,309
GCN4_YEAST_Staller_2018	Binding	4	617	44	2021
SPG1_STRSG_Wu_2016	Binding	2	2167	4	147,193
CAPSD_AAV2S_Sinai_2021	Organismal Fitness	1	532	28	41,796
HIS7_YEAST_Pokusaeva_2019	Organismal Fitness	2	1643	28	494,494

Table 8: Summary of ProteinGym datasets used for alignment.

	Avg	D7PM05	GFP	Q6WV12	Q8WTC7	GCN4	SPG1	CAPSD	HIS7
KERMUT	0.628	0.820	0.764	0.843	0.773	0.461	0.227	0.494	0.645
ConFit	0.679	0.871	0.829	0.845	0.800	0.250	0.460	0.714	0.585
ProGen3-46B	0.673	0.825	0.837	0.798	0.706	0.339	0.451	0.753	0.672

Table 9: Supervised fitness prediction performance of different methods.

ConFit also performs similarly on CAPSD_AAV2S_Sinai_2021, but KERMUT has meaningfully worse performance on this assay (Table 9).

For the other three assays, there is no such correlation between model scale and fitness prediction performance, though using a larger model almost never causes a meaningful performance drop. This suggests that IRPO learns most effectively from rich single-mutation data, and that on balance, larger models benefit more from alignment than smaller models. Each of the baseline methods also has noticeably worse performance than ProGen3-46B on two of these three assays (Table 9).

We also observe that the two assays where all methods obtain the worst performance (GCN4_YEAST_Staller_2018 and SPG1_STRSG_Wu_2016) both measure binding affinity. Given that the pre-training data contains no signals about a protein's binding partner, predicting a protein's binding affinity is likely a challenging task for models of this sort. However, access to richer single-mutation data may still improve performance for this task.

E Split-GFP Methods and Supporting Information

E.1 Competent cell preparation

Two days in advance, *E. coli* BLl-21 DE3 (either with or without p15a-GFP$_{1\text{-}10}$) was struck onto LB agar with or without kanamycin 50 μg/L, and incubated overnight at 37°C. One day in advance, a single colony was inoculated into 50 mL LB with or without kanamycin 50 μg/L in a 250 mL shake flask, and incubated overnight at 37°C 225 RPM. On the day of, the overnight pre-culture was inoculated 1:100 into 500 mL to 2L LB with or without kanamycin 50 μg/mL in 2L shake flasks, and incubated at 37°C 225 RPM, until OD600 was between 0.4 and 0.6. The flasks were then chilled for 30 minutes on ice and then pelleted by centrifugation (10min, 3500 RCF, 4°C) in chilled 500mL plastic centrifuge bottles. The supernatant was decanted and pellets were suspended in TFB I (100 mM rubidium chloride, 50 mM manganese chloride (MnCl2 H20), 30 mM potassium acetate, 10 mM calcium chloride (CaCl2H2O), 15% v/v glycerol) at a ratio of 1:10 TFBI to starting culture volume. Resuspended cells were incubated on ice for 15 minutes and then pelleted by centrifugation (10min, 3500 RCF, 4°C). The supernatant was decanted and pellets were suspended in TFB II (10mM 3-(N-morpholino)propanesulfonic acid (MOPS), 10mM rubidium chloride, 75 mM calcium chloride, 15% glycerol) at a ratio of 1:25 TFBII to starting culture volume. The resuspensions were

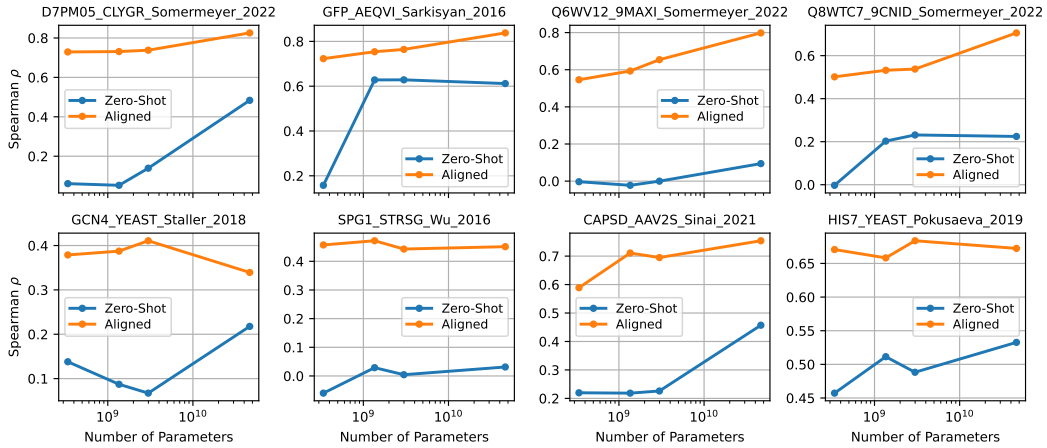

Figure 6: Fitness prediction by zero-shot and aligned models on the assays described in Table 8.

incubated on ice for 30 minutes, before being gently homogenized by inversion, and aliquoted to 96w plates, before storage at -80°C.

E.2 Cloning of expression plasmid backbones

The expression plasmids for the PoI-GFP$_{11}$ and GFP$_{1\text{-}10}$, pTet-PoI-GFP$_{11}$ and p15a-GFP$_{1\text{-}10}$, respectively, were modeled after Cabantous 2005, synthesized by Twist Bioscience with overlapping fragments, assembled via NEB HiFi following manufacturer recommendations, transformed into 10-beta competent *E. coli* (New England Bioscience), and plated on LB agar containing the appropriate antibiotic. Colonies were picked, miniprepped (Zymo), and sequence verified via long-read nanopore sequencing (Plasmidsaurus) (Table 10).

E.3 Cloning of the GFP11 fusion libraries

The PoI insert libraries were codon optimized for *E. coli* with DNA Chisel [111], flanked with BsaI Type II restriction sites and synthesized as gene fragments via Twist Bioscience. Plate maps were specified such that generated and wild type proteins from the same cluster were located on the same plate. Positive and negative controls (human dihydrofolate reductase DHFR, NP_000782.1, and human GPCR beta-3 adrenergic receptor, NP_000016.1, respectively) were added to each plate. Additionally, several wells were left empty on each plate to permit background subtraction at the fluorescent measurement stage. DNA fragments were suspended in 100 μL H20. BsaI-HFv2 Golden Gate reactions were performed using manufacturer recommendations (New England Bioscience) scaled to 10 μL per assembly. Golden Gate reactions consisted of 30 cycles X (5 min 37°C, 5 min 16°C) followed by 5 min 60°C. 5 μL completed Golden Gate reaction was transformed following manufacturer recommendations into BL-21 DE3 competent cells either with or without p15a-GFP$_{1\text{-}10}$ (New England Bioscience). Transformations were plated onto LB agar plates containing 75 μg/L spectinomycin either with or without 50 μg/L kanamycin using a Hamilton liquid handler. Up to four colonies per assembly were picked using a Qpix robotic colony picker into liquid LB containing 75 μg/L spectinomycin with or without 50 μg/L kanamycin. Colony PCR was performed using primers splitgpf-PoI-fwd and splitgpf-PoI-rv (Table 11) and RedTaq PCR mastermix (Thermo Fischer) following manufacturer recommendations, scaled to 10 μL. To spot check, PCR reactions were diluted 1:40 in water and size-verified by capillary electrophoresis (Revvity LabChip).

E.4 Sequence verification

For each plate of assemblies, we generated an in silico pool of references sequences, corresponding to the PCR amplicons using primers splitgpf-PoI-fwd and splitgpf-PoI-rv (Table 11). Prior to sequencing, all pools were pre-validated to ensure sufficient sequence diversity using Jellyfish with kmer size set to 31 [64]. A custom Python script was run across the resulting kmer file to ensure each member of the pool had a kmer with a sufficient edit distance from all other members of the pool.

Plasmid	DNA Sequence 2
pTet-PoI-GFP$_{11}$	ccgccgccctagacctagggcgttcggctgcggcgagcggtatcagctcactcaaaggcggtaatacggttatccacagaatcaggggataacgcaggaaagaacatgtgagcaaaaggccagcaaaaggccaggaaccgtaaaaaggccgcgttg ctggcgttttccataggctccgcccccctgacgagcatcacaaaaatcgacgctcaagtcagaggtggcgaacccgacaggactataaagatacccaggcgtttccccctggaagctccctcgtgcgctctcctgttccgaccctgcgcttaccggata cctgtccgcctttctcccttcgggaagcgtggcgctttctcatagctcacgctgtaggtatctcagttcggtgtaggtcgttcgctccaagctgggctgtgtgcacgaaccccccgttcagcccgaccgctgcgccttatccggtaactatcgtcttgagtccaa cccgtaagacacgacttatcgccactggcagcagccactggtaacaggattagcagagcgaggtatgtaggcggtgctacagagttcttgaagtggtggcctaactacggctacactagaaggacagtatttggtatctgcgctctgctgaagccagtta ccttcggaaaaaagagttggtagctcttgatccggcaaacaaaccaccgctggtagcggtggtttttttgtttgcaagcagcagattacgcgcagaaaaaaaggatctcaagaagatcctttgatcttttctacggggtctgacgctcagtggaacgaaaactca cgttaaggatttggtcatgactagcgcttggattctcaccaataaaaacgcccggcggcaaccgagcgttctgaacaaatccagatggagttctgaggtcattactgatctatcaacaggagtccaagcttaagacccacttcacattaagttgttttct aatccgtatatgatcaattcaaggccgaataagaaggctggctctgcaccttggtgatcaaataattcgatagcttgtcgtaataatggcggcatactatcagtagtaggtgtttccctttctcttttgcgactgatgctctgatctcccataacgcaacctaaagt aaaatgcccacagcgctgagtgcataataatgcattctctagtgaaaaacctttgtggcataaaaaggctaattgatttttcgagagtttcatactgttttctgtaggccgtgtacctaaatgtacttttgctccatcgcgatgacttagtaaagcatctaaaacttt agcgttattacgtaaaaaatttgcagctttcccctctaaaggggcaaaagtgagtatggtgcctatctaacatctcaatggccaaggcgtcgagcaatgcccgcttattttttacatgcaatacaatgtaggctgctctacacctagcttctggtgagtttacg ggttgttaaacctttcgattccgacctcattaagcagctctaatgcgctgttaatcactttacttttatctaatctgagacatcattaatgtttattgagctctcgaacccccagagtcccgcattatttgccgactacctggtgatctcgcctttcacgtagtggacaaattct tccaactgatctgcgcgcgaggccaagcgatcttcttcttgtccaagataagcctgtctagcttcaagtatgacgggctgatactgggccggcaggcgctccattgcccagtcggcagcgacatccttcggcgcgattttgccggttactgcgctgtaccaaa tgcgggacaacgtaagcactacatttcgctcatcgccagcccagtcgggcggcgagttccatagcgttaaggtttcattttagcgcctcaaatagatcctgttcaggaaccggatcaaagagttcctccgccgctggacctaccaaggcaacgctatgttctct tgctttgtcagcaagatagccagatcaatgtcgatcgtggctggctcgaagatacctgcaagaatgtcattgcgctgccattctccaaattgcagttcgcgcttagctggataacgccacggaatgatgtcgtgcgtgcacaacaatggtgacttctacagcgc ggagaatctcgctctctccaggggaagccgaagtttccaaaaggtcgttgatcaaagctcgccgcgttgtttcatcaagccttacggtcaccgtaaccagcaaatcaatatcactgtgtggcttcaggccgccatccactgcggagccgtacaaatgtacgg ccagcaacgtcggttcgagatggcgctcgatgacgccaactacctctgatagttgagtcgatacttcggcgatcaccgcttccctcatgatgtttaacttgttttagggcgactgcccctgctgcgtaacatcgttgctgctccataacatcgaacatcgacccac ggcgtaacgcgcttgctgcttggatgcccgaggcatagactgtaccccaaaaaaacagtcataacaagccatgaaaaccgccactgcgccgttaccatgcgaaacgatcctcatcctgtctctttgatcagatcttgatcccctgcgccatcagatccttggc ggcaagaaagccatccagtttactttgcagggcttcccaacctaccagagggcgccccagctggcaattccgacgtctaagaaaccattattatcatgacattaacctataaaaataggcgtatcacgaggccctttcgtcttcacctcgagtcccatcagtg atagagattgacatccctatcagtgatagagatactgagcacatcagcaggacgcactgaccggttcattaaagaggagaaagatacctATGTGAGACCTAATTAATTAATTGGTCTCAGGATCCGATGGAGG GTCTGGTGGCGGATCAACAAGTCGTGACCACATGGTCCTTCATGAGTACGTAAATGCTGCTGGGATTACATAAGGTACCTAACTCGAGTGAGATCCGGCT GCTAACAAAGCCCGAAAGGAAGCTGAGTTGGCTGCTGCCACCGCTGAGCAATAACTAGCATAACCTCTAGAGGCCtaacaaataaacgaaaggctcagtcgaaagactgggc cttcgttttatctgttgtttgtcggtgaacgctctcctgagtaggacaaat
p15a-GFP$_{1\text{-}10}$	TTTCCAGTCGGGAAACCTGTCGTGCCAGCTGCATTAATGAATCGGCCAACGCGCGGGGAGAGGCGGTTTGCGTATTGGGCGCCAGGGTGGTTTTTCTTTT CACCAGTGAGACGGGCAACAGCTGATTGCCCTTCACCGCCTGGCCCTGAGAGAGTTGCAGCAAGCGGTCCACGCTGGTTTGCCCCAGCAGGCGAAAATC CTGTTTGATGGTGGTTAACGGCGGGATATAACATGAGCTGTCTTCGGTATCGTCGTATCCCACTACCGAGATATCCGCACCAACGCGCAGCCCGGACTCG GTAATGGCGCGCATTGCGCCCAGCGCCATCTGATCGTTGGCAACCAGCATCGCAGTGGGAACGATGCCCTCATTCAGCATTTGCATGGTTTGTTGAAAAC CGGACATGGCACTCCAGTCGCCTTCCCGTTCCGCTATCGGCTGAATTTGATTGCGAGTGAGATATTTATGCCAGCCAGCCGACACGCCGCGCGAGAC AGAACTTAATGGGCCCGCTAACAGCGCGATTTGCTGGTGACCCAATGCGACCAGATGCTCCACGCCCAGTCGCGTACCGTCTTCATGGGAGAAAATAATA CTGTTTGATGGGTGTCTGGTCAGAGACATCAAGAAATAACGCCGGAACATTAGTCAGCAGCTTTGCACAGCAATGGCATCCTGGTCATCCAGCGGATAG TTAATGATCAGCCCACTGACGCGTTGCGCGAGAAGATTGTGCACCGCCGCTTTACAGGCTTCGACGCCGCTTCGTTCTACCATCGACACCACCACGCTGG CACCCAGTTGATCGGCGCGAGATTTAATCGCCGCGACAATTTGCGACGGCGCGTGCAGGGCCAGACTGGAGGTGGCAACGCCAATCAGCAACGACGTGTT TGCCCGCCAGTTGTTGTGCCACGCGGTTGGGAATGTAATTCAGCTCCGCCATCGCCGCTTCCACTTTTTCCCGCGTTTTCGCAGAAACGTGGCTGGCCTGG TTCACCACGCGGGAAACGGTCTGATAAGAGACACCGGCATACTCTGCGACATCGTATAACGTTACTGGTTTCACATTCACCACCCTGAATTGACTCTCTTC CGGGCGCTATCATGCCATACCGCGAAAGGTTTTGCGCCATTCGATGGTGTCCGGGATCTCGACGCTCTCCCTTATGCGACTCCTGCATTAGGAAGCAGCC CAGTAGTAGGTTGAGGCCGTTGAGCACCGCCGCCGCAAGGAATGGTGCATGCAAGGAGATGGCGCCCAACAGTCCCCCGGCCACGGGGCCTGCCACCAT ACCCACGCCGAAACAAGCGCTCATGAGCCCGAAGTGGCGAGCCCGATCTTCCCCATCGGTGATGTCGGCGATATAGGCGCCAGCAACCGCACCTGTGGC GCCGGTGATGCCGGCCACGATGCGTCCGGCGTAGAGGATCGAGATCTCGATCCCGCGAAATTAATACGACTCACTATAGGGGAATTGTGAGCGGATAAC AATTCCCCTCTAGGATCCGAATTCGAGCTCTCTAGAGAAAGAGGAGAAATACTAGATGAGCAAAGGAGAAGAACTTTTCACTGGAGTTGTCCCAATTCTT GTTGAATTAGATGGTGATGTTAATGGGCACAAATTTTCTGTCAGAGGAGAGGGTGAAGGTGATGCTACAATCGGAAAACTCACCCTTAAATTTATTTGCA CTACTGGAAAACTACCTGTTCCATGGCCAACACTTGTCACTACTCTGACCTATGGTGTTCAATGCTTTTCCCGTTATCCGGATCACATGAAAAGGCATGAC TTTTTCAAGAGTGCCATGCCCGAAGGTTATGTACAGGAACGCACTATATCTTTCAAAGATGACGGGAAATACAAGACGCGTGCTGTAGTCAAGTTTGAAG GTGATACCCTTGTTAATCGTATCGAGTTAAAGGGTACTGATTTTAAAGAAGATGGAAACATTCTCGGACACAAACTCGAGTACAACTTTAACTCACACAA TGTATACATCACGGCAGACAAACAAAAGAATGGAATCAAAGCTAACTTCACAGTTCGCCACAACGTTGAAGATGGTTCCGTTCAACTAGCAGACCATTAT CAACAAAATACTCCAATTGGCGATGGGCCCTGTCCTTTTACCAGACAACCATTACCTGTCGACACAAACTGTCCTTTCGAAAGATCCCAACGAAAAGTAAA AGCTTGCGGCCGCACTCGAGCACCACCACCACCACCACTGAGATCCGGCTGCTAACAAAGCCCGAAAGGAAGCTGAGTTGGCTGCTGCCACCGCTGAGC AATAACTAGCATAACCCCTTGGGGCCTCTAAACGGGTCTTGAGGGGTTTTTTGCTGAAAGGAGGAACTATATCCGGATTGGCGAATGGGACGCGCCCTGT AGCGGCGCATTAAGCGCGGCGGGTGTGGTGGTTACGCGCAGCGTGACCGCTACACTTGCCAGCGCCCTAGCGCCCGCTCCTTTCGCTTTCTTCCCTTCCTT TCTCGCCACGTTCGCCGGCTTTCCCCGTCAAGCTCTAAATCGGGGGCTCCCTTTAGGGTTCCGATTTAGTGCTTTACGGCACCTCGACCCCAAAAAACTTG ATTAGGGTGATGGTTCACGTAGTGGGCATCGCCCTGATAGACGGTTTTTCGCCCTTTGACGTTGGAGTCCACGTTCTTTAATAGTGGACTCTTGTTCCAA ACTGGAACAACACTCAACCCTATCTCGGTCTATTCTTTTGATTTATAAGGGATTTTGCCGATTTCGGCCTATTGGTTAAAAAATGAGCTGATTTAACAAAA ATTTAACGCGAATTTTAACAAAATATTAACGCTTACAATTTAGGTGGCACTTTTCGGGGAAATGTGCGCGGAACCCCTATTTGTTTATTTTTCTAAATACA TTCAAATATGTATCCGCTCATGAATTAATTCTTAGAAAAACTCATCGAGCATCAAATGAAACTGCAATTTATTCATATCAGGATTATCAATACCATATTTT TGAAAAAGCGTTTCTGTAATGAAGGAGAAAACTCACCGAGGCAGTTCCATAGGATGGCAAGATCCTGGTATCGGTCTGCGATTCCGACTCGTCCAACAT CAATACAACCTATTAATTTCCCCTCGTCAAAAATAAGGTTATCAAGTGAGAAATCACCATGAGTGACGACTGAATCCGGTGAGAATGGCAAAAGTTTATG CATTTCTTTCCAGACTTGTTCAACAGGCCAGCCATTACGCTCGTCATCAAAATCACTCGCATCAACCAAACCGTTATTCATTCGTGATTGCGCCTGAGCGA GACGAAATACGCGATCGCTGTTAAAAGGACAATTACAAACAGGAATCGAATGCAACCGGCGCAGGAACACTGCCAGCGCATCAACAATATTTTCACCTG AATCAGGATATTCTTCTAATACCTGGAATGCTGTTTTCCCGGGGATCGCAGTGGTGAGTAACCATGCATCATCAGGAGTACGGATAAAATGCTTGATGGT CGGAAGAGGCATAAATTCCGTCAGCCAGTTTAGTCTGACCATCTCATCTGTAACATCATTGGCAACGCTACCTTTGCCATGTTTCAGAAACAACTCTGGCG CATCGGGCTTCCCATACAATCGATAGATTGTCGCACCTGATTGCCCGACATTATCGCGAGCCCATTTATACCCATATAAATCAGCATCCATGTTGGAATTT AATCGCGGCCTAGAGCAAGACGTTTCCCGTTGAATATGGCTCATAACACCCCTTGTATTACTGTTTATGTAAGCAGACAGTTTTATTGTTTGcgcacaattatatcg tatgggctgacttcaggtgctacattgaagagataaattgcactgaaatctagaaatattttatctgattaataaagatgatcttcttgagatcgttttggtctgcgcgtaatctcttgctctgaaaacgaaaaaccgccttgcagggcggttttcgaaggttctct gagctaccaactctttgaaccgaggtaactggcttggaggagcgcagtcaccaaaacttgtccttcagtttagcctaaccggcgcatgacttcaagactaactcctctaaatcaattaccagtggctgctgccagtggtgcttttgcatgtcttccgggttgg actcaagacgatagttaccggataaggcgcagcggtcggactgaacgggggttcgtgcatacagtccagcttggagcgaactgcctacccggaactgagtgtcaggcgtggaatgagacaaacgcggccataacagcggaatgacaccggtaaac cgaaaggcaggaacaggagagcgcacgagggagccgccagggggaaacgcctggtatctttatagtcctgtcgggtttcgccacctctgacttgagcgtcgatttttgtgatgcttgtcaggggggcggagcctatggaaaacggctttgccgcggc cctctcacttccctgttaagtatcttcctggcatcttccaggaaatctccgcccctgtcgtaagccatttccgctgccgcagtcgaacgaccgagcgtagcgagtcagtgagcgaggaagcggaatatatcctgtatcacatattctgcatgcacccggtgc agcctttttctcctgccacatgaagcaacttcactgacacctcatcagtgccaacatagtaagccagtatacactccgctagcgcactagtTTGCTCAGGTCGCAGACGTTTTGCAGCAGCAGTCGCTTCACGTTC GCTCGCGTATCGGTGATTCATTCTGCTAACCAGTAAGGCAACCCCGCCAGCCTAGCCGGGTCCTCAACGACAGGAGCACGATCATGCGCACCCGTGGGGC CGCCATGCCGGCGATAATGGCCTGCTTCTCGCCGAAACGTTTGGTGCGCGGGACCCAGTGACGCAAGGGCTGAGCGAGGGCGTGCAAGATTCCGAATACCGC AAGCGACAGGCCGATCATCGTCGCGCTCCAGCGAAAGCGGTCCTCGCCGAAAATGACCCAGAGCGCTGCCGGCACCTGTCCTACGAGTTGCATGATAAA GAAGACAGTCATAAGTGCGGCGACGATAGTCATGCCCCGCGCCCACCGGAAGGAGCTGACTGGGTTGAAGGCTCTCAAGGGCATCGGTCGAGATCCCGG TGCCTAATGAGTGAGCTAACTTACATTAATTGCGTTGCGCTCACTGCCCGC

Table 10: Plasmids used in this study.

Plasmid	DNA Sequence 2
splitgpf-PoI-fwd	gcaggacgcactgaccgagttc
splitgpf-PoI-rv	agggcggcggatttgtcctact

Table 11: Primers used for the size and sequence validation of PoI inserts in pTet-PoI-GFP$_{11}$.

PCR reactions were pooled, size-selected (1x v:v Beckman Coulter Ampure beads, 2x 80% ethanol wash), and sequenced via Oxford Nanopore PromethION sequencing using R10.4.1 flow cells (Plasmidsaurus). For each sequenced pool, Plasmidsaurus returned a single FASTQ containing all reads. Reference amplicons of the expected library members were compiled into a multi-FASTA. The FASTQ and reference FASTA went through the following analysis steps: All unique 31-mers per reference sequence were identified by Uniquekmer [17]. Reads were filtered based on length. Reads with fewer than 50 bp were discarded using BBDuk [10]. Reads were demultiplexed based on exact match to unique 31-mers using BBSeal [10]. Demultiplexed reads were mapped to reference sequences using minimap2 [58]. Consensus sequence generated based on aligned reads using samtools [25]. Variants were called between the consensus and the reference using DNADiff [54]. Colonies were filtered for sequence fidelity, coverage, and depth (>10 reads covering the ORF), and a single correct representative of each genotype was hitpicked using a Hamilton liquid handler. Hitpick plates were grown overnight in liquid LB containing 75 μg/L spectinomycin with or without 50 μg/L kanamycin, mixed 1:1 with 50% glycerol, and stored at -80°C until assay.

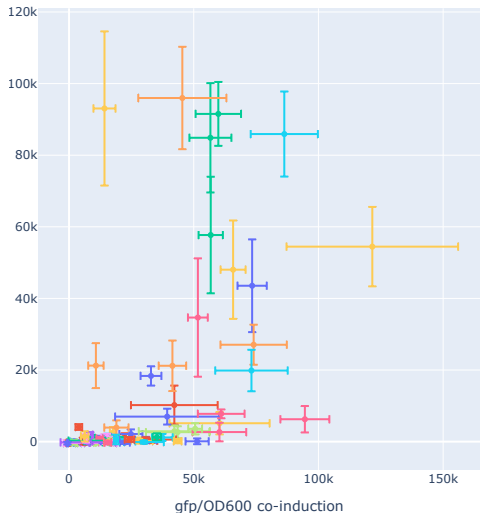

Figure 7: Scatter plot of mean split-GFP under sequential induction (y-axis) vs mean co-induction (x-axis), t = 16 hours, for 91 unique proteins. Each color is a unique protein sequence. Error bars are standard deviation of n = 4 replicates.

E.5 Split-GFP Assay

In general, the preparation and assay of the PoIs and GFP1-10 and assay followed the protocols delineated in Cabantous, 2006 [11]. The split-GFP assay can be either run in cells using two orthogonal expression plasmids, or in lysate. In a pilot study, we observed a poor correlation between the two methods ($r^2 = -0.27$, $n = 91$ proteins), and that SDS-PAGE abundance was better correlated with GFP fluorescence under sequential induction (Figures 7–9). We further validated the sequential induction approach with SDS-PAGE of 88 proteins (Figure 10). Although the relatively high limit of detection for SDS-PAGE prevents quantitative correlation across the range of measured GFP values, we observed excellent identification of highly expressing and lowly expressing proteins. 19 of 23 proteins in the top quartile had distinct bands at the correct size, while 22 of 22 proteins in the bottom quartile had no detectable band (Figure 8). In the top quartile, two bands were absent. The other two proteins without proper migration were two highly-expressing proteins that failed to migrate on the gel, implying high stability or resistance to SDS-mediated denaturation (Figure 10). While boiling (up to 100°C, 10 min) or proteinase K treatment afforded partial purification, neither led to proper migration of the bands. Interestingly, both of these proteins shared the same cluster with the most closely related natural protein 3-hydroxyacyl-[acyl-carrier-protein] dehydratase FabZ.

Due to the higher correlation with SDS-PAGE, we chose the in-lysate approach for experimental validation of the broader set. We describe both approaches in more detail below.

E.5.1 Whole-cell assay

Glycerol stocks containing pTet-PoI-GFP$_{11}$ and p15a-GFP$_{1\text{-}10}$ plasmids were inoculated into 1 mL liquid LB containing 75 μg/L spectinomycin and 50 μg/liter kanamycin sulfate and grown overnight in a shaking plate incubator (37°C, 1000RPM). In the morning, overnight growth was inoculated in quadruplicate plates 1:100 in LB containing 75 μg/L spectinomycin and 50 μg/liter kanamycin sulfate, and grown in a shaking plate incubator (37°C, 1000RPM) until OD600 reached 0.5 to 1.0. PoI-GFP$_{11}$ expression was induced by the addition of anhydrotetracycline in ethanol to a final concentration of 250 ng/L. Simultaneous GFP$_{1\text{-}10}$ was induced by the addition of isopropyl β-D-thiogalactopyranoside (IPTG) to a final concentration of 0.1 mM. Protein production continued for two hours in a shaking incubator (37°C, 1000RPM). Cultures were diluted 1:1 in LB to a final volume of 100 μL in a 384-well black clear bottom plate (Greiner 781097). Fluorescence and OD600 were read on a Tecan Spark plate reader (Ex: 475nm, Em: 530 nm, Gain: 69, Z-position: 30000).

E.5.2 Lysate assay

Preparation of protein of interest: Glycerol stocks containing pTet-PoI-GFP11 plasmids were inoculated into 1mL liquid LB containing 75 μg/L spectinomycin and grown overnight in a shaking plate incubator (37°C, 1000RPM). In the morning, overnight growth was inoculated 1:50 in quadruplicate in 1mL LB containing 75 μg/L spectinomycin, and grown in a shaking plate incubator (37°C, 1000RPM) until OD600 reached 0.5 to 1.0. PoI was induced by the addition of anhydrotetracycline in ethanol to a final concentration of 250 ng/L. Protein production continued for two hours in a shaking incubator (37°C, 1000RPM). Culture-containing plates were spun down (3500 RCF, 5 minutes), decanted, and 100 μL BugBuster MasterMix (EMD Millipore) containing 25 μg/mL chloramphenicol was added to lyse cells and stop protein expression. Cells were lysed by incubation in a shaking incubator (25°C, 300RPM, 1 hour). Lysates were stored overnight at 4° before assay.

Preparation of GFP1-10 p15a-$GFP_{1\text{-}10}$ was transformed into *E. coli* BL-21 DE3 competent cells (New England Bioscience) following manufacturer recommendations. A single colony was grown overnight in LB 50 μg/liter kanamycin sulfate, diluted 1:1 with 50% glycerol, and stored at -80°C. Biomass from the glycerol stock was inoculated into 50 mL LB 50 μg/liter kanamycin sulfate in a 250 mL shake flask, and incubated overnight (37°C, 225 RPM). The following morning, the overnight culture was inoculated 1:100 into LB 50 μg/liter kanamycin sulfate in a 2 L shake flask. After two hours (37°C, 225 RPM), $GFP_{1\text{-}10}$ expression was induced with a final concentration of 1 mM isopropyl β-D-thiogalactopyranoside (IPTG). After five hours of incubation (37°C, 225 RPM), the culture was placed at 4° and left overnight. The following morning, the culture was spun down (3500 RCF x 15 minutes) and re-suspended in 1/5 of the culture volume (i.e. 200 mL for 1 L culture) in lysis buffer containing 100 mm Tris HCl Ph 7.5, 10% glycerol, and 150 mm sodium chloride (TNG buffer). The resuspended culture was sonicated on ice (VWR 76193-590 50% duty, 10 minutes, 30 second pulse). The lysate was centrifuged (3500 RCF x 15 minutes) and the $GFP_{1\text{-}10}$-containing supernatant was decanted.

E.5.3 In trans folding and fluorescence measurement

10 μL of PoI-$_{GFP11}$ lysate were added to 90uL of the $GFP_{1\text{-}10}$ lysate in a 384-well black clear bottom plate (Greiner 781097). Plates were sealed and incubated at 25°C overnight. Fluorescence was read on a Tecan Spark plate reader (Ex: 475nm, Em: 530 nm, Gain: 69, Z-position 30000). Samples were background subtracted using the mean fluorescence of the empty wells on a per plate basis.

E.6 SDS-PAGE validation

10 μL of cell lysate were diluted with 30 μL BugBuster Protein Extraction Reagent with 25 μg/mL chloramphenicol and then added to 12 μL Laemmli + DTT and pipet mixed. Samples were heated at 85°C for 3 min. 10 μL were loaded on a Mini-PROTEANő TGX Precast Gel (BioRad) and run at 120V for 50 minutes. Gels were rinsed in DI water then opened and transferred into troughs filled with DI water. Troughs were gently shaken for 15 minutes on an Ohaus light duty orbital shaker at 130 rpm at room temperature. Then DI water was replaced and this wash process was repeated two more times. Gels were then stained with GelCode Blue Stain Reagent for 45 minutes while shaking at 130 rpm. Gel was de-stained by decanting dye and adding DI water and shaking at 130 rpm for another hour. Photographs were taken via smartphone camera.

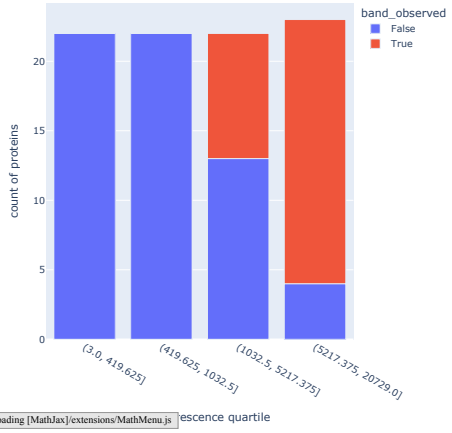

Figure 8: Count of SDS-PAGE bands observed at correct size for 92 proteins, organized by GFP quartile.

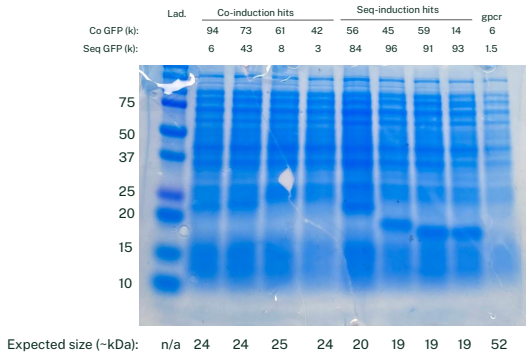

Figure 9: SDS-PAGE of 9 proteins. Top rows show mean GFP fluorescence in either co- or sequential induction experiments, t = 16 hours. The bottom row shows expected size in kDa.

Sample:	ladder	A1	B1	C1	D1	E1	F1	G1	H1	-ctrl
GFP:		1545.5	1031	302.5	2268.5		339	366	2886.5	
kDA:		13.9	15.1	26	21.2		31.6	15.9	15.6	
Band obs:		false	false	false	false		false	false	false	

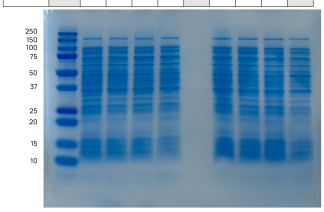

Sample:	A2	lad	B2	C2	D2	D2	F2	G2	H2	-ctrl
GFP:	1022.5		343.5	2118.5	2405.5	14816	340	566.5	696.5	
kDA:	14.7		15.5	14.9	15.8	33.6	30.6	32.5	17.8	
Band obs:	false		false	false	true	true	false	false	false	

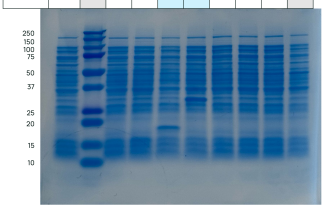

Sample:	A3	B3	lad	C3	D3	E3	F3	G3	H3	-ctrl
GFP:	796.5	2461		19576	10244	14737	778.5	650	585.5	
kDA:	32.0	20.0		15.3	18.7	17.7	15.7	14.5	17.8	
Band obs:	false	false		true	false*	true	false	false	false	

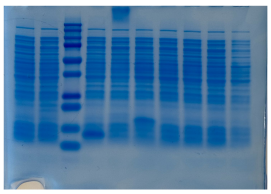

Sample:	A4	B4	C4	lad	D4	E4	F4	G4	H4	-ctrl
GFP:	518.5	359.5	17784		580	345.5	2564.5	428.5	382	
kDA:	22.8	18.4	16.8		29.4	19.0	15.2	42.7	17.8	
Band obs:	false	false	true		false	false	false	false	false	

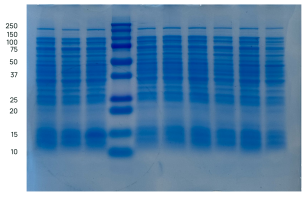

Sample:	A5	B5	C4	D5	lad	E5	F5	G5	H5	-ctrl
GFP:	6279.5	17596	5062	5239.5		347.5	447.5	3786	4304	
kDA:	18.8	19.0	18.0	14.0		19.6	15.3	18.0	14.9	
Band obs:	true	true	false	false		false	false	true	true	

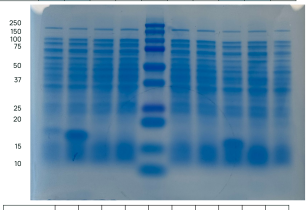

Sample:	A6	B6	C6	D6	E6	lad	F6	G6	H6	-ctrl
GFP:	2684	1034	334	17663	12682		423	4297	390	
kDA:	31.6	17.8	38.1	14.8	19.0		18.3	15.4	18.4	
Band obs:	true	true	false	true	false		false	true	false	

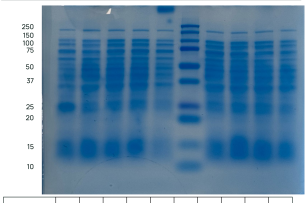

Sample:	A7	B7	C7	D7	E7	F7	lad	G7	H7	-ctrl
GFP:	13668.5	5151	341.5	288.5	646.5	16409.5		2629.5	426.5	
kDA:	32.7	33.1	31.5	17.4	32.4	18.0		14.7	31.5	
Band obs:	true	false	false	false	false	true		true	false	

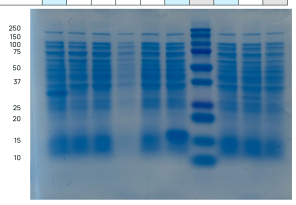

Sample:	A8	B8	C8	D8	E8	F8	G8	lad	H8	-ctrl
GFP:	3865.5	1971.5	361.5	1098	423	506.5	10635		11356.5	
kDA:	18.8	14.3	22.2	21.6	30.3	15.7	32.4		31.6	
Band obs:	false	false	false	true	false	false	false		true	

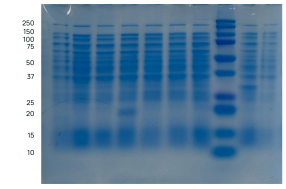

Sample:	lad	A9	B9	C9	D9	E9	F9	G9	H9	-ctrl
GFP:		472	390.5	3652	13437.5	418.5	587.5	7304.5	254.5	
kDA:		32.8	14.7	15.7	33.0	34.0	33.3	14.5	31.2	
Band obs:		false	false	true	true	false	false	true	false	

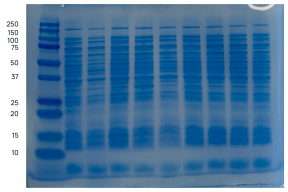

Sample:	A10	lad	B10	C10	D10	E10	F10	G10	H10	-ctrl
GFP:	864.5		385.5	5893	9518	8563	17329	1083	2251	
kDA:	14.7		18.1	18.2	14.5	14.1	28.0	14.9	17.5	
Band obs:	false		false	true	true	true	true	false	false	

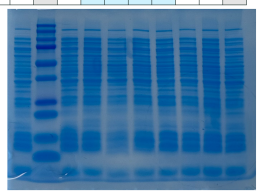

Sample:	A11	B11	lad	C11	D11	E11	F11	G11	H11	-ctrl
GFP:	1005	1856		20729	12347	356.5	12056	336.5	333.5	
kDA:	33.3	34.3		14.9	14.1	27.8	30.5	27.7	12.4	
Band obs:	false	false		true	true	false	true	false	false	

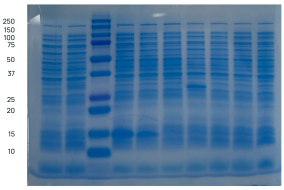

Sample:	A12	B12	-rl	lad
GFP:	267.5	581.5		
kDA:	46.2	24.1		
Band obs:	false	false		

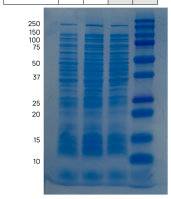

Figure 10: SDS-PAGE gels of induced proteins. Each lane is labeled by plate position, background-subtracted GFP, and boolean call on band presence at the anticipated size. Negative control is un-induced plasmid.